Abstracta

Ano XXIX - N. 01

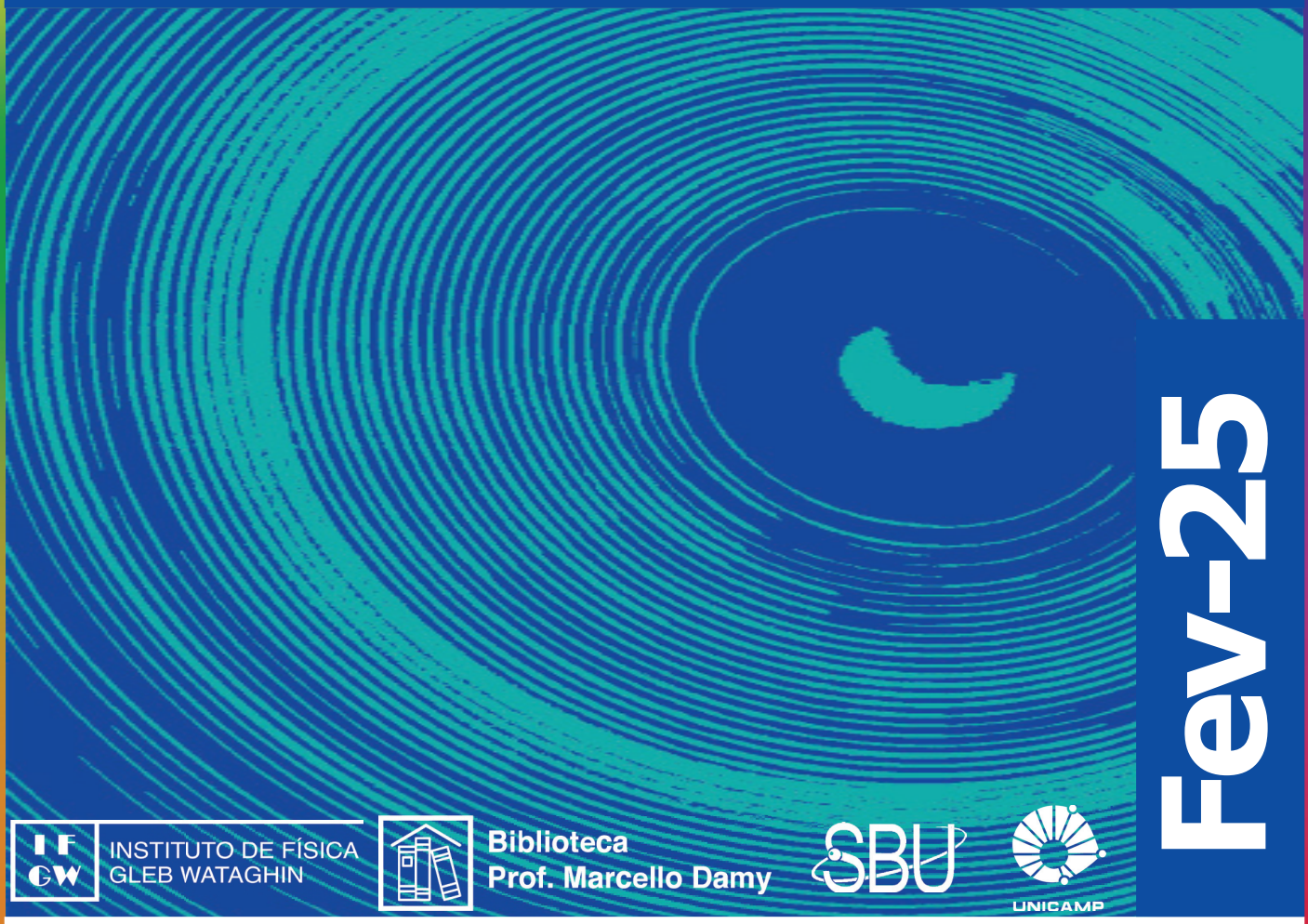

Artigos publicados 2024 - P320-2024 à P398-2024

Artigos publicados 2025 - P001-2025 à P025-2025

Defesas de Dissertações do IFGW - D002-2025 à D005-2025

Defesas de Teses do IFGW - T002-2025 à T004-2025

Artigos publicados 2024

[P320-2024] "Azimuthal anisotropy of jet particles in p-Pb and Pb-Pb collisions at √sNN=5.02 TeV"

Acharya, S.; Adamová, D.; Adler, A.; **Chinellato, D. D.*; Guardiano, G. G.*; Jahnke, C.*; Takahashi, J.*;** et al.
ALICE Collaboration

The azimuthal anisotropy of particles associated with jets (jet particles) at midrapidity is measured for the first time in p-Pb and Pb-Pb collisions at root sNN = 5.02 TeV down to transverse momentum (p(T)) of 0.5 GeV/c and 2 GeV/c, respectively, with ALICE. The results obtained in p-Pb collisions are based on a novel three-particle correlation technique. The azimuthal anisotropy coefficient v(2) in high-multiplicity p-Pb collisions is positive, with a significance reaching 6.8 sigma at low p(T), and its magnitude is smaller than in semicentral Pb-Pb collisions. In contrast to the measurements in Pb-Pb collisions, the v(2) coefficient is also found independent of p(T) within uncertainties. Comparisons with the inclusive charged-particle v(2) and with AMPT calculations are discussed. The predictions suggest that parton interactions play an important role in generating a non-zero jet-particle v(2) in p-Pb collisions, even though they overestimate the reported measurement. These observations shed new insights on the understanding of the origin of the collective behaviour of jet particles in small systems such as p-Pb collisions, and provide significant stringent new constraints to models.

JOURNAL OF HIGH ENERGY PHYSICS [8], 234, 2024. DOI: 10.1007/JHEP08(2024)234

[P321-2024] "Bifurcations in the Kuramoto model with external forcing and higher-order interactions"

Costa, G. S.; **Novaes, M.*; de Aguiar, A. M.***

Synchronization is an important phenomenon in a wide variety of systems comprising interacting oscillatory units, whether natural (like neurons, biochemical reactions, and cardiac cells) or artificial (like metronomes, power grids, and Josephson junctions). The Kuramoto model provides a simple description of these systems and has been useful in their mathematical exploration. Here, we investigate this model by combining two common features that have been observed in many systems: External periodic forcing and higher-order interactions among the elements. We show that the combination of these ingredients leads to a very rich bifurcation scenario that produces 11 different asymptotic states of the system, with competition between forced and spontaneous synchronization. We found, in particular, that saddle-node, Hopf, and homoclinic manifolds are duplicated in regions of parameter space where the unforced system displays bi-stability.

CHAOS 34[12], 123133, 2024. DOI: 10.1063/5.0239011

[P322-2024] "Chaotic orbital dynamics of pulsating stars around black holes surrounded by dark matter halos"

Amancio, T. S.*; Mosna, R. A.*; Vieira, R. S. S.

We analyze the orbital dynamics of spherical test bodies in "black hole surrounded by dark matter halo" spherically symmetric spacetimes. When the test body pulsates periodically (such as a variable star), altering its quadrupole tensor, Melnikov's method shows that its orbital dynamics presents homoclinic chaos near the corresponding unstable circular orbits however small the oscillation amplitude is. Since for supermassive black holes the period of revolution of a star near the innermost stable circular orbit roughly spans time intervals from minutes to hours, the formalism can be applied in principle to the astrophysical scenario of a pulsating (variable) star inspiraling into a supermassive black hole, including the black hole SgrA* at the center of our Galaxy. The chaotic nature of its orbit, due to pulsation, is imprinted in the redshift time series of the emitted light and can, in principle, be observed in the corresponding light curves and even in gravitational-wave signals detected by future observatories such as the Laser Inteferometer Space Antenna. Also, although periodic with respect to the star's proper time, the chaotic orbital motion will produce an erratic light curve (and gravitational-wave signal) in terms of observed, coordinate time. Although our results were obtained for a specific exact solution, we argue that this phenomenon is generic for pulsating bodies immersed in black hole spacetimes surrounded by self-gravitating fluids.

PHYSICAL REVIEW D 110[12], 124048, 2024. DOI: 10.1103/PhysRevD.110.124048

[P323-2024] "Combination of the TD-DFT and the pixel counting method for determining electron capture cross sections for protons impacting on organic molecules"

Oliveira, L. A. de*; Farias, J. C. de*; Bernal, M. A.*

The electron capture by heavy charged particles is of interest in a wide range of physical applications. In radiation biophysics, electron capture cross sections (ECCS) is a key information for the implementation of Monte Carlo simulation codes. In this work, the time-dependent density functional theory (TD-DFT) has been used for the determination of ECCS for protons impacting on atoms with presence in organic compounds, in the 1-200 keV energy range. Later, these atomic cross sections were combined through the pixel counting method for determining corresponding cross section of small and large organic molecules and water, which is of primordial importance in radiation biophysics. The large organic molecules include DNA bases and a whole DNA base pair. Excellent results were obtained for the small molecules along the whole energy range. For DNA components, good results were found at high energies (100-200 keV). At lower energies, larger discrepancies were obtained when compared with other theoretical and experimental work. The possible causes for these discrepancies are deeply discussed. This work should support later works for developing a charge equalization method for classical molecular dynamics to describe fast proton collisions with organic materials.

EUROPEAN PHYSICAL JOURNAL D 78[12], 147, 2024. DOI: 10.1140/epjd/s10053-024-00939-y

[P324-2024] "Comparative evaluation of collagen modifications in breast cancer in human and canine carcinomas"

Garcia, A. P. V.; Reis, L. A.; Ribeiro, B. R. M.; Nunes, C. B.; **Paula, A. M. de***; Cassali, G. D.

New diagnostic and therapeutic approaches have been increasingly demanded due to the high morbidity and mortality associated with breast cancer. Recently, changes in the collagen fibres in mammary neoplasms have been shown to provide information that can be helpful for more accurate diagnosis. We aimed to conduct a comparative analysis of the tumour stroma in human and canine mammary neoplasms to assess the relationship between collagen modifications and the behaviour of carcinomas in both species, by multiphoton microscopy. We present a retrospective study of 70 cases of human mammary tumour and 74 cases of canine mammary tumour. We analysed sections stained with haematoxylin and eosin from 1,200 representative areas of normal mammary tissue, fibroadenoma, grade I invasive carcinoma, grade III invasive carcinoma and invasive micropapillary carcinoma in human species and 1,304 representative areas of normal mammary tissue,

benign mixed tumour, mixed carcinoma, carcinosarcoma, invasive micropapillary carcinoma and solid carcinoma in canine species. We obtained that both human and canine mammary carcinomas present lower density of collagen fibres, higher density of cells and the collagen fibres are more aligned than in normal tissue. For human mammary carcinomas, the collagen fibres are more linear as compared to normal tissue. In addition, we demonstrated that the carcinomas with unfavourable prognosis present shorter collagen fibres, and these collagen changes correlate with the clinical and pathological data in human and canine species. For dogs, there is a correlation between the mean fibre length with the specific survival times. Thus, we demonstrate that dogs provide an excellent comparative perspective for studying how changes in the tumour stroma affect patient survival.

SCIENTIFIC REPORTS 14[1], 28846, 2024. DOI: 10.1038/s41598-024-79854-6

[P325-2024] "Dark energy survey year 3 results: likelihood--free, simulation-based wCDM inference with neural compression of weak-lensing map statistics"

Jeffrey, N.; Whiteway, L.; Gatti, M.; Williamson, J.; Alsing. J.; **Navarro-Alsina, A.*;** et al.

We present simulation-based cosmological wcold dark matter (wCDM) inference using dark energy survey year 3 weak-lensing maps, via neural data compression of weak-lensing map summary statistics: power spectra, peak counts, and direct map-level compression/inference with convolutional neural networks (CNN). Using simulation-based inference, also known as likelihood-free or implicit inference, we use forward-modelled mock data to estimate posterior probability distributions of unknown parameters. This approach allows all statistical assumptions and uncertainties to be propagated through the forward-modelled mock data; these include sky masks, non--Gaussian shape noise, shape measurement bias, source galaxy clustering, photometric redshift uncertainty, intrinsic galaxy alignments, non-Gaussian density fields, neutrinos, and non--linear summary statistics. We include a series of tests to validate our inference results. This paper also describes the Gower Street simulation suite: 791 full-sky pkdgrav3 dark matter simulations, with cosmological model parameters sampled with a mixed active-learning strategy, from which we construct over 3000 mock dark energy survey lensing data sets. For wCDM inference, for which we allow -1<w<-(1)(3), our most constraining result uses power spectra combined with map--level (CNN) inference. Using gravitational lensing data only, this map-level combination gives Omega(m)=0.283(-0.027)(+0.020), S-8=0.804(-0.017)(+0.025), and w<-0.80 (with a 68 per cent credible interval); compared to the power spectrum inference, this is more than a factor of two improvement in dark energy parameter (Omega(DE),w) precision.

MONTHLY NOTICES OF THE ROYAL ASTRONOMICAL SOCIETY 536[2], p.1303-1322, 2024. DOI: 10.1093/mnras/stae2629

[P326-2024] "Development of a SiPM-Based Water-Cherenkov Detector for Astrophysics"

Fauth, A. C.*; Machado, A. A.*; Pimentel, V. D.; **Segreto, E.*; dos Santos, R. F.***

The Cherenkov effect is widely employed in experiments involving cosmic rays and neutrinos that utilize large sensitive volumes. The water is widely employed as the sensitive medium, with the primary particle to be detected being the muon. In this work, we present the development of a new water-Cherenkov detector that utilizes a photon trapping system and silicon photomultipliers (SiPMs) to record the detector signals, which has been named C-Arapuca. The utilization of SiPMs presents advantages over the traditional photomultiplier tube, PMT, such as a much lower operating voltages and the construction of more compact devices with greater geometric freedom. To study the performance of the C-Arapuca, a tank containing 550 L of ultra-pure water was utilized. The confinement of Cherenkov photons is achieved through a dichroic filter in the optical window and a light guide that shifts the photons wavelength and guide them to the eight SiPMs positioned along its sides. The results of the efficiency of muon detection from local cosmic radiation are presented, indicating the feasibility of employing the C-Arapuca in future astroparticle experiments.

ASTRONOMISCHE NACHRICHTEN, e20240123, 2024. DOI: 10.1002/asna.20240123 Early Access Date: NOV 2024

[P327-2024] "Development of the CMS detector for the CERN LHC Run 3"

Hayrapetyan, A.; Tumasyan, A.; Adam, W.; **Chinellato, J. A.***; et al.
CMS Collaboration

Since the initial data taking of the CERN LHC, the CMS experiment has undergone substantial upgrades and improvements. This paper discusses the CMS detector as it is configured for the third data-taking period of the CERN LHC, Run 3, which started in 2022. The entire silicon pixel tracking detector was replaced. A new powering system for the superconducting solenoid was installed. The electronics of the hadron calorimeter was upgraded. All the muon electronic systems were upgraded, and new muon detector stations were added, including a gas electron multiplier detector. The precision proton spectrometer was upgraded. The dedicated luminosity detectors and the beam loss monitor were refurbished. Substantial improvements to the trigger, data acquisition, software, and computing systems were also implemented, including a new hybrid CPU/GPU farm for the high-level trigger.

JOURNAL OF INSTRUMENTATION 19[5], P05064, 2024. DOI: 10.1088/1748-0221/19/05/P05064

[P328-2024] "Doping liquid argon with xenon in ProtoDUNE Single-Phase: effects on scintillation light"

Abud, A. A; Abi, B.; Acciarri, R.; **Adriano, C.*; Bazetto, M. C. Q.*; Borges Merlo, R.*; Aguiar, R. de*; Almeida, P. de*; Holanda, P. C. de*; Gelli, B.*; Giammaria, P.*; Gratieri, D. R.*; Guzzo, M. M.*; Kemp, E.*; Machado, A. A.*; Marques, F. das C.*; Peres, O. L. G.*; Pimentel, V. L.*; Prakash, S.*; Segreto, E.***; et al.
DUNE Collaboration

Doping of liquid argon TPCs (LArTPCs) with a small concentration of xenon is a technique for light-shifting and facilitates the detection of the liquid argon scintillation light. In this paper, we present the results of the first doping test ever performed in a kiloton-scale LArTPC. From February to May 2020, we carried out this special run in the single-phase DUNE Far Detector prototype (ProtoDUNE-SP) at CERN, featuring 720 t of total liquid argon mass with 410 t of fiducial mass. A 5.4 ppm nitrogen contamination was present during the xenon doping campaign. The goal of the run was to measure the light and charge response of the detector to the addition of xenon, up to a concentration of 18.8 ppm. The main purpose was to test the possibility for reduction of non-uniformities in light collection, caused by deployment of photon detectors only within the anode planes. Light collection was analysed as a function of the xenon concentration, by using the pre--existing photon detection system (PDS) of ProtoDUNE-SP and an additional smaller set-up installed specifically for this run.

In this paper we first summarize our current understanding of the argon-xenon energy transfer process and the impact of the presence of nitrogen in argon with and without xenon dopant. We then describe the key elements of ProtoDUNE-SP and the injection method deployed. Two dedicated photon detectors were able to collect the light produced by xenon and the total light. The ratio of these components was measured to be about 0.65 as 18.8 ppm of xenon were injected. We performed studies of the collection efficiency as a function of the distance between tracks and light detectors, demonstrating enhanced uniformity of response for the anode-mounted PDS. We also show that xenon doping can substantially recover light losses due to contamination of the liquid argon by nitrogen.

JOURNAL OF INSTRUMENTATION 19[8], P08005, 2024. DOI: 10.1088/1748-0221/19/08/P08005

[P329-2024] "Emergent symmetries of relativistic fluid dynamics from local ergodicity"

Torrieri, G.*

We show that volume-preserving diffeomorphisms and the chemical shift symmetry defining relativistic Lagrangian ideal fluid dynamics can be derived as an emerging symmetry when ergodicity is assumed to apply locally in a way that is invariant under smooth spacetime foliations. This can be used as a way to derive the ideal hydrodynamic limit in a strongly coupled but strongly fluctuating medium. We comment on the connection with thermalization in small systems, the eigenstate thermalization hypothesis and deviations from the ideal limit.

PHYSICAL REVIEW D 109[5], L051903, 2024. DOI: 10.1103/PhysRevD.109.L051903

[P330-2024] "Evidence for tWZ production in proton-proton collisions at $\sqrt{s}$=13 TeV in multilepton final states"

Hayrapetyan, A.; Tumasyan, A.; Adam, W.; **Chinellato, J. A.***; et al.
CMS Collaboration

The first evidence for the standard model production of a top quark in association with a W boson and a Z boson is reported. The measurement is performed in multilepton final states, where the Z boson is reconstructed via its decays to electron or muon pairs. At least one W boson, associated or from top quark decay, decays leptonically, too. The analysed data were recorded by the CMS experiment at the CERN LHC in 2016-2018 in proton-proton collisions at root s = 13 TeV, and correspond to an integrated luminosity of 138 fb(-1). The measured cross section is 354 +/- 54(stat) +/- 95(syst) fb, and corresponds to a statistical significance of 3.4 standard deviations.

PHYSICS LETTERS B 855, 138815, 2024. DOI: 10.1016/j.physletb.2024.138815

[P331-2024] "Experimental and theoretical insights on the influence of substrate oscillation period on advanced coatings deposited by dynamic glancing angle deposition"

Jimenez, M. J. M.*; Leidens, L. M.*; Boeira, C. D.*; Antunes, V. G.*; Cemin, F.*; Riul Jr, A.*; Zagonel, L. F.*; Figueroa, C. A.; **Wisnivesky, D.*;** Zanatta, A. R.; **Alvarez, F.***

Dynamic Glancing Angle Deposition (DGLAD) was explored to tune the properties of chromium nitride (CrN) hard coatings, addressing the unexplored impact of short oscillation periods (1 < T < 10 min) on film properties. The study revealed that substrate oscillation significantly influences microstructure, creating a distinctive wavy, columnar microstructure. Atomic Force Microscopy (AFM) and Scanning Electron Microscopy (SEM) showed unique morphological and texture changes in oscillated samples when compared to a sample deposited under the same conditions but in stationary geometry (without oscillation). Mechanical properties such as residual strain, hardness, and crystallite size were also notably affected by the oscillation period. Simulations offered insights into precursor atom flux dynamics, linking oscillation conditions to property variation. This method opens new paths for enhancing the durability and performance of hard coatings in industrial applications with the precise control of properties.

JOURNAL OF MATERIALS RESEARCH, 2024. DOI: 10.1557/s43578-024-01501-7 Early Access Date: DEC 2024

[P332-2024] "Exploring the electronic and mechanical properties of the recently synthesized nitrogen-doped amorphous monolayer carbon"

Santos, E. J. A.; Pereira Junior, M. L.; Tromer, R. M.; **Galvao, D. S.*;** Ribeiro Junior, L. A.

The recent synthesis of nitrogen-doped amorphous monolayer carbon (NAMC) opens new possibilities for multifunctional materials. In this study, we have investigated the nitrogen doping limits and their effects on NAMC's structural and electronic properties using density functional-based tight-binding simulations. Our results show that NAMC remains stable up to 35% nitrogen doping, beyond which the lattice becomes unstable. The formation energies of NAMC are higher than those of nitrogen-doped graphene for all the cases we have investigated. Both undoped MAC and NAMC exhibit metallic behavior, although only MAC features a Dirac-like cone. MAC has an estimated Young's modulus value of about 410 GPa, while NAMC's modulus can vary around 416 GPa depending on nitrogen content. MAC displays optical activity in the ultraviolet range, whereas NAMC features light absorption within the infrared and visible ranges, suggesting potential for distinct optoelectronic applications. Their structural thermal stabilities were addressed through molecular dynamics simulations. MAC melts at approximately 4900 K, while NAMC loses its structural integrity for temperatures ranging from 300 K to 3300 K, lower than graphene. These results point to potential NAMC applications in flexible electronics and optoelectronics.

NANOSCALE, 2024. DOI: 10.1039/d4nr04305g Early Access Date: DEC 2024

[P333-2024] "Exploring the Electronic and Mechanical Properties of TPDH Nanotube: Insights from Ab Initio and Classical Molecular Dynamics Simulations"

Quispe, J. G.; **Galvao, D. S.***; Autreto, P. A. D.

Tetra-Penta-Deca-Hexa graphene (TPDH) is a new two-dimensional (2D) carbon allotrope with attractive electronic and mechanical properties. It is composed of tetragonal, pentagonal, decagonal and hexagonal carbon rings. When TPDH graphene is sliced into quasi-one-dimensional (1D) structures such as nanoribbons, it exhibits a range of behaviors, from semimetallic to semiconducting. An alternative approach to achieving these desirable electronic properties (electronic confinement and nonzero electronic band gap) is the creation of nanotubes (TPDH-NTs). In the present work, we carried out a comprehensive study of TPDH-NTs combining Density Functional Theory (DFT) and classical reactive Molecular Dynamics (MD). Our results show structural stability and a chiral dependence on the mechanical properties.

Similarly to standard carbon nanotubes, TPDH-NT can be metallic or semiconductor. MD results show Young's modulus values exceeding 700 GPa, except for nanotubes with very small radii. However, certain chiral TPDH-NTs (n, m) display values both below and above 700 GPa, particularly for those with small radii. Analysis of the evolution of von Mises stress and the distribution of C-C bond angles and lengths throughout the stress-strain process indicates the important role of tetragonal, pentagonal, and hexagonal rings for the mechanical response of TPDH-NTs. Tetragonal and pentagonal rings provide a rigid mechanical framework for TPDH-NTs (n, 0), whereas pentagonal and hexagonal rings provide TPDH-NTs (0, n) with greater flexibility.

ACS OMEGA 9[51], p.50225- 50236, 2024. DOI: 10.1021/acsomega.4c05614

[P334-2024] "Exploring the Strong Interaction of Three--Body Systems at the LHC"

Acharya, S.; Adamová, D.; Rinella, G. A.; **Chinellato, D. D.*; Guardiano, G. G.*; Jahnke, C.*; Liveraro, G. S. S.*; Takahashi, J.*;** et al.
ALICE Collaboration

Deuterons are atomic nuclei composed of a neutron and a proton held together by the strong interaction. Unbound ensembles composed of a deuteron and a third nucleon have been investigated in the past using scattering experiments, and they constitute a fundamental reference in nuclear physics to constrain nuclear interactions and the properties of nuclei. In this work, Kthorn-d and p-d femtoscopic correlations measured by the ALICE Collaboration in proton-proton (pp) collisions at root s = 13 TeV at the Large Hadron Collider (LHC) are presented. It is demonstrated that correlations in momentum space between deuterons and kaons or protons allow us to study three-hadron systems at distances comparable with the proton radius. The analysis of the Kthorn-d correlation shows that the relative distances at which deuterons and protons or kaons are produced are around 2 fm. The analysis of the p-d correlation shows that only a full three-body calculation that accounts for the internal structure of the deuteron can explain the data. In particular, the sensitivity of the observable to the short-range part of the interaction is demonstrated. These results indicate that correlations involving light nuclei in pp collisions at the LHC will also provide access to any threebody system in the strange and charm sectors.

PHYSICAL REVIEW X 14[3], 031051, 2024. DOI: 10.1103/PhysRevX.14.031051

[P335-2024] "First measurement of the total inelastic cross section of positively charged kaons on argon at energies between 5.0 and 7.5 GeV"

Abud, A. A.; Abi, B.; Acciarri, R.; **Adriano, C.*; Bazetto, M. C. Q.*; Borges Merlo, R.*; De Aguiar, R.*; De Almeida, P.*; De Holanda, P. C.*; Gelli, B.*; Gratieri, D. R.*; Guzzo, M. M.*; Kemp, E.*; Machado, A. A.*; Das Chagas Marques, F.*; Peres, O. L. G.*; Pimentel, V. L.*; Porto Paixao, L. G.*; Segreto, E.* ;** et al.
DUNE Collaboration

ProtoDUNE Single-Phase (ProtoDUNE-SP) is a 770-ton liquid argon time projection chamber that operated in a hadron test beam at the CERN Neutrino Platform in 2018. We present a measurement of the total inelastic cross section of charged kaons on argon as a function of kaon energy using 6 and 7 GeV/c beam momentum settings. The flux-weighted average of the extracted inelastic cross section at each beam momentum setting was measured to be 380 +/- 26 mbarns for the 6 GeV/c setting and 379 +/- 35 mbarns for the 7 GeV/c setting.

PHYSICAL REVIEW D 110[9], 092011, 2024. DOI: 10.1103/PhysRevD.110.092011

[P336-2024] "FLUORESCENCE SPECTROSCOPY: FROM FUNDAMENTALS TO THE INFLUENCE OF INSTRUMENTAL PARAMETERS FOR ANALYSIS OF ORGANIC DYES AND INORGANIC NANOPARTICLES"

Mourao, R. S.; **Vale, B. R. C.***; Fonseca, A. F. V.; Carvalho, T. A. S.; Schiavon, M. A.

Fluorescence spectroscopy is an extremely sensitive analytical technique that has been widely used to elucidate problems that require low detection limits. Although fluorescence spectroscopy is widespread in industry and academia, there is a lack of teaching materials demonstrating its basic principles, as well as the influence of instrumental parameters involved in the technique, which limit its correct use and the full potential of it. For this reason, this work aims to explore the principles of fluorescence spectroscopy and correlate them in function of different instrumental variables to carry out a fluorescence experiment. The spectrofluorometer parameters such as the excitation wavelength, excitation and emission slits, step, integration time, detection geometry as well as concentration of the samples were varied to illustrate how the best resulting spectra can be registered free of artifacts. To do so, two organic dyes with structured vibronic bands (pyrene) and another with unstructured bands (rhodamine 6G) were used. Another study carried out involved the use of 3D spectra, excitation/emission spectra, of cadmium telluride (CdTe) quantum dots. In this case, it was possible to show the excitation spectrum of nanomaterials, collecting emissions at different wavelengths, as well as analyzing the particle size distribution.

QUIMICA NOVA 47[2], 2024. DOI: 10.21577/0100-4042.20230095

[P337-2024] "Global Room-Temperature Superconductivity in Graphite"

Kopelevich, Y.*; Torres, J.*; Silva, R. O. F. da*; Diamantini, M. C.; Trugenberger, C.; Vinokur, V.

Room temperature superconductivity under normal conditions has been a major challenge of physics and material science since its discovery. Here the global room-temperature superconductivity observed in cleaved highly oriented pyrolytic graphite carrying dense arrays of nearly parallel surface line defects is reported. The multiterminal measurements performed at the ambient pressure in the temperature interval 4.5 K <= T <= 300 K and at magnetic fields 0 <= B <= 9 T applied perpendicular to the basal graphitic planes reveal that the superconducting critical current I-c(T, B) is governed by the normal state resistance R-N(T, B) so that I-c(T, B) is proportional to 1/R-N(T, B). Magnetization M(T, B) measurements of superconducting screening and hysteresis loops together with the critical current oscillations with temperature that are characteristic for superconductor-ferromagnet-superconductor Josephson chains, provide strong support for the occurrence of superconductivity at T > 300 K. A theory of global superconductivity emerging in the array of linear structural defects is developed which well describes the experimental findings and demonstrate that global superconductivity arises as a global phase coherence of superconducting granules in linear defects promoted by the stabilizing effect of underlying Bernal graphite via tunneling coupling to the three dimensional (3D) material.

ADVANCED QUANTUM TECHNOLOGIES 7[2], 2024. DOI: 10.1002/qute.202300230

[P338-2024] "Hadronic rescattering to solve the helicity puzzle in B plus -* ppπ+ (K plus) decays"

Bediaga, I.; Shalchi, M. A.; Frederico, T.; **Magalhaes, P. C.***

We explore the contribution of hadronic final state interactions (FSI) to propose a production mechanism and interpret the puzzle on helicity angle distributions in B+ -* p p<overline>,r+ and B+ -* pp<overline>K+ decays. Experimental results indicate opposite helicity angle 6p distributions in those two channels with the difference presenting a remarkable linear dependence on cos 6p. We assume the production mechanism is driven by B+ -* xym+ -* pp<overline>m+, where m = ,r or K, and xy represents favorable mesonic decay channels producing p p<overline>. We develop a model that includes a three-body final state interaction between the p, p<overline>, and ,r+ or K+ considering the dominance of elastic channels ,r+p and K+ p<overline> interactions below 2 GeV/c2. Our three-body framework with FSI explains qualitatively the observed opposite behavior of the helicity distributions and the observed linearity.

PHYSICAL REVIEW D 110[9], 096026, 2024. DOI: 10.1103/PhysRevD.110.096026

[P339-2024] "Hole doping and electronic correlations in Cr substituted BaFe2As2"

Cantarino, M. D.; **Pakuszewski, K. R.***; Salzmann, B.; Moya, P. H. A.; Neto, W. R. D.; **Freitas, G. S.*; Pagliuso, P. G.*; Adriano, C*** Brito, W. H.; Garcia, F. A.

For a significant composition range, the suppression of the spin density wave transition temperature (T SDW) in Cr- and Mn--substituted BaFe2As2 (CrBFA and MnBFA, respectively) coincides as a function of Cr/Mn content, despite the distinct electronic effects of these substitutions. Additionally, for any Cr/Mn content superconductivity (SC) is absent and this topic is particularly less explored in the case of CrBFA. In this work, we employ angle- resolved photoemission spectroscopy (ARPES) and combined density functional theory plus dynamical mean field theory (DFT+DMFT) to address the evolution of the Fermi surface (FS) and electronic correlations in CrBFA. Our findings reveal that incorporating Cr leads to an effective hole doping of the states near the FS, which is well described within the virtual crystal approximation (VCA). Moreover, analysis of the ARPES spectra of the bands with main d ye--orbital character reveals a fractional scaling of the imaginary part of self-energy as a function of the binding energy, a signature property of Hund's correlations. Our DFT+DMFT calculations support these experimental findings. We conclude that CrBFA is a correlated electron system for which the changes in the FS as a function of Cr are unrelated to the suppression of T SDW In addition, we suggest that the absence of SC is primarily due to the competition between Cr local moments and the Fe-derived itinerant spin fluctuations.

SCIPOST PHYSICS 17[5], 141, 2024. DOI: 10.21468/SciPostPhys.17.5.141

[P340-2024] "Impact of the magnetic horizon on the interpretation of the Pierre Auger Observatory spectrum and composition data"

Halim, A. A.; Abreu, P.; Aglietta, M.; **Arbeletche, L. B.*; Chinellato, J. A.*; Dobrigkeit, C.*; Fauth, A. C.*; Payeras, A. M.*; Akim, J. V. R.*;** et al.
Pierre Auger Collaboration

The flux of ultra-high energy cosmic rays reaching Earth above the ankle energy (5 EeV) can be described as a mixture of nuclei injected by extragalactic sources with very hard spectra and a low rigidity cutoff. Extragalactic magnetic fields existing between the Earth and the closest sources can affect the observed CR spectrum by reducing the flux of low-rigidity particles reaching Earth. We perform a combined fit of the spectrum and distributions of depth of shower maximum measured with the Pierre Auger Observatory including the effect of this magnetic horizon in the propagation of UHECRs in the intergalactic space. We find that, within a specific range of the various experimental and phenomenological systematics, the magnetic horizon effect can be relevant for turbulent magnetic field strengths in the local neighbourhood in which the closest sources lie of order B-rms similar or equal to (50-100) nG(20Mpc/ds)(100 kpc/L--coh)(1/2), with d(s) the typical intersource separation and L--coh the magnetic field coherence length. When this is the case, the inferred slope of the source spectrum becomes softer and can be closer to the expectations of diffusive shock acceleration, i.e., proportional to E-2. An additional cosmic-ray population with higher source density and softer spectra, presumably also extragalactic and dominating the cosmic-ray flux at EeV energies, is also required to reproduce the overall spectrum and composition results for all energies down to 0.6 EeV.

JOURNAL OF COSMOLOGY AND ASTROPARTICLE PHYSICS [7], 094, 2024. DOI: 10.1088/1475-7516/2024/07/094

[P341-2024] "Influence of Methylammonium Chloride on Wide-Bandgap Halide Perovskites Films for Solar Cells"

Guaita, M. G. D.; Szostak, R.; **Silva, F. M. C. da***; Morais, A. de; Moral, R. F.; Kodalle, T.; Teixeira, V. C.; Sutter-Fella, C. M.; Tolentino, H. C. N.; Nogueira, A. F.

Wide-bandgap perovskites are of paramount importance as the photoactive layer of the top cell in high-efficiency tandem solar cells. Comparably high Br contents are required to widen the perovskite bandgap. However, the increase in Br content causes heterogeneous halide distribution and photoinstability. Here, the positive effect of the additive methylammonium chloride (MACl) on the optical and electronic properties of Br-rich perovskite, deposited using N-methyl-2-pyrrolidone (NMP) as co-solvent and the gas quenching method, is investigated. Simultaneous in situ grazing-incidence wide-angle X-ray scattering and photoluminescence spectroscopy are used to track the evolution of the structural and optoelectronic properties of the perovskites with different amounts of Br and MACl during the spin-coating and thermal annealing steps. The formation mechanism is elucidated in the presence of MACl. It is observed that chloride ions inhibit the intermediate phases, favoring the formation of a perovskite phase with higher crystallinity. Nano X-ray fluorescence mapping recognizes Br-richer and poorer nanometric domains, whose average sizes reduce for samples with MACl. In conclusion, it is demonstrated that adding MACl affects the formation of wide-bandgap perovskites via destabilization of the intermediate phases and acts on the homogenization of the halide distribution, leading to improved solar cell performances.Wide-bandgap perovskites are relevant materials for tandem cells. However, the addition of bromine, to increase the bandgap, leads to the formation of a perovskite richer in defects, with halide distribution heterogeneity and photoinstability. Here, the study of the impact and mode of action of methylammonium chloride (MACl) additive, shows the inhibition of intermediates formation and the halide distribution homogenization with MACl.image

ADVANCED FUNCTIONAL MATERIALS 34[50], SI, 2024. DOI: 10.1002/adfm.202307104

[P342-2024] "Intermittent migration can induce pulses of speciation in a two-island system"

Princepe, D.*; Czarnobai, S.; Caetano, R. A.; **Marquitti, F. M. D.*; de Aguiar, M. A. M.***; Araujo, S. B. L.

Geographic barriers can come and go depending on natural conditions. These fluctuations cause population cycles of expansion and contraction, introducing intermittent migrations that may not hinder speciation but rather promote diversification. Here, we study a neutral 2-island speciation model with intermittent migration driven by sea-level fluctuations. Seabed depth modulates isolation and connection periods between the islands, with migration occurring during connection periods with a certain probability. Mating is restricted to genetically compatible individuals on the same island and offspring inherit genomes from both parents through recombination. We observe speciation pulses that would not occur under strict isolation or continuous migration, with infrequent, temporary increases in species richness happening at different times depending on the combination of geographic settings and migration probability. The resulting dynamic patterns of richness exhibit contrasting behavior between connected and isolated scenarios, often including species that do not persist. Prolonged isolation can reduce richness to 1 species per island, resembling patterns commonly associated with archipelagos under sea-level fluctuations. Together with other studies, our results in out-of-equilibrium populations support the relevance of investigating the impact of variable migration on diversification, particularly in regions of high diversity.

EVOLUTION 78[4], 758-767, 2024. DOI: 10.1093/evolut/qpad210

[P343-2024] "Internalization and Cellular Fate of Protein Corona-Coated Nanoparticles by Multimodal Multi-Scale Microscopy"

Galdino, F. E.;* Rabelo, R. S.; **Scarpa, I.***; Yoneda, J. S.; **Consonni, S. R.*; Leme, A. F. P.***; Smith, A. M.; Harkiolaki, M.; Cardoso, M. B.

Upon exposure to biological environments, nanoparticles are rapidly coated with biomolecules, predominantly proteins, which alter their colloidal stability, biodistribution, and cell interactions. Despite extensive efforts to investigate the nanoparticles' fate, only a few studies use high-resolution characterization methods that allow in-depth characterization, and the existing methodologies are unable to differentiate particles internalized at the onset of incubation from those taken up toward the end of an incubation period. In this study, these limitations related to incubation disparities are overcame and precisely monitored the spatiotemporal displacement of colloidally stable protein corona-coated nanoparticles within cells. An unprecedented application of cryogenic X-ray nanotomography, combined with high-resolution, super-resolution, and correlative microscopy techniques, revealed the migration of nanoparticles to the perinuclear region while monitoring the evolution of cellular organelles in fully hydrated cells under near-native conditions, without the need for contrasting agents. Notably, this tracking indicates the progressive fusion of vesicles carrying the nanoparticles intracellularly. This strategy demonstrates the potential for uncovering the temporal aspects of nanoparticle behavior within cells and can be adaptable to a wide range of nanoparticles and cell types, offering a versatile and powerful tool to follow nanoparticles in cellular environments.

SMALL, 2024. DOI: 10.1002/smll.202409065 Early Access Date: DEC 2024

[P344-2024] "Intrinsic Coexistence of Miscibility and Segregation in Gold-Silver Nanoalloys"

Moreira, M.*; Cottancin, E.; Pellarin, M.; Roiban, L.; Masenelli-Varlot, K.; **Ugarte, D.*; Rodrigues, V.*; Hillenkamp, M.***

Bimetallic nanoparticles are used in numerous applications in catalysis, plasmonics or fuel cell technology. The addition of the second metal to the nanoparticles allows enhancing and fine-tuning their properties by choosing their composition, size, shape and environment. However, the crucial additional parameter of chemical structure within the particle is difficult to predict and access experimentally, even though segregated core-shell structures and random alloys can have drastically different physicochemical properties. This is highlighted by the vast literature on the most studied bimetallic system, gold-silver, for which the controversy on whether gold and silver are miscible on the nanoscale or segregate persists. Here, these contradictions are solved by determining quantitatively the coexistence of an alloyed core and a 1-2 nm thick shell with gradual silver enrichment as the chemical ground state structure. Chemical reactions with the environment and meta-stable structures are furthermore identified as responsible for the contradictions in the literature. This method is applicable to other multi-metallic systems, provides benchmark input for theoretical models, and forms the basis for studying chemical rearrangements under reactive conditions in catalysis.

SMALL, 2024. DOI: 10.1002/smll.202411151 Early Access Date: DEC 2024

[P345-2025] "Investigating strangeness enhancement in jet and medium via φ(1020) production in p-Pb collisions at √sNN=5.02 TeV"

Acharya, S.; Adamova, D.; Agarwal, A.; **Chinellato, D. D.*; Guardiano, G. G.*; Liveraro, G. S. S.*; Takahashi, J.*;** et al. ALICE Collaboration

This work aims to differentiate strangeness produced from hard processes (jetlike) and softer processes (underlying event) by measuring the angular correlation between a high-momentum trigger hadron (h) acting as a jet proxy and a produced strange hadron [f(1020) meson]. Measuring h-phi correlations at midrapidity in p-Pb collisions at root s(NN) = 5.02 TeV as a function of event multiplicity provides insight into the microscopic origin of strangeness enhancement in small collision systems. The jetlike and the underlying-event-like strangeness production are investigated as a function of event multiplicity. They are also compared between a lower and higher momentum region. The evolutions of the per-trigger yields within the near-side (aligned with the trigger hadron) and away-side (in the opposite direction of the trigger hadron) jets are studied separately, allowing for the characterization of two distinct jetlike production regimes. Furthermore, the h-phi correlations within the underlying event give access to a production regime dominated by soft production processes, which can be compared directly to the in-jet production. Comparisons between h-phi and dihadron correlations show that the observed strangeness enhancement is largely driven by the underlying event, where the phi/h ratio is significantly larger than within the jet regions. As multiplicity increases, the fraction of the total phi(1020) yield coming from jets decreases compared to the underlying event production, leading to high-multiplicity events being dominated by the increased strangeness production from the underlying event.

PHYSICAL REVIEW C 110[6], 064912, 2024. DOI: 10.1103/PhysRevC.110.064912

[P346-2024] "Investigating strangeness enhancement with multiplicity in pp collisions using angular correlations"

Acharya, S.; Adamová, D.; Agarwal, A.; **Chinellato, D. D.*; Guardiano, G. G.*; Liveraro, G. S. S.*; Takahashi, J.*;** et al. ALICE Collaboration

A study of strange hadron production associated with hard scattering processes and with the underlying event is conducted to investigate the origin of the enhanced production of strange hadrons in small collision systems characterised by large charged-particle multiplicities. For this purpose, the production of the single-strange meson K-S(0) and the double-strange baryon Xi is measured, in each event, in the azimuthal direction of the highest-p(T) particle ("trigger" particle), related to hard scattering processes, and in the direction transverse to it in azimuth, associated with the underlying event, in pp collisions at root s = 5.02 TeV and root s = 13 TeV using the ALICE detector at the LHC. The per-trigger yields of K-S(0) and Xi(+/-) are dominated by the transverse-to-leading production (i.e., in the direction transverse to the trigger particle), whose contribution relative to the toward-leading production is observed to increase with the event charged-particle multiplicity. The transverse-to-leading and the toward-leading Xi(+/-)/K-S(0) yield ratios increase with the multiplicity of charged particles, suggesting that strangeness enhancement with multiplicity is associated with both hard scattering processes and the underlying event. The relative production of Xi(+/-) with respect to K-S(0) is higher in transverse-to-leading processes over the whole multiplicity interval covered by the measurement. The K-S(0) and Xi(+/-) per-trigger yields and yield ratios are compared with predictions of three different phenomenological models, namely PYTHIA8.2 with the Monash tune, PYTHIA8.2 with ropes and EPOS LHC. The comparison shows that none of them can quantitatively describe either the transverse--to-leading or the toward-leading yields of K-S(0) and Xi(+/-).

JOURNAL OF HIGH ENERGY PHYSICS [9], 204, 2024. DOI: 10.1007/JHEP09(2024)204

[P347-2024] "Investigating the composition of the K0*(700) state with π±KS0 correlations at the LHC"

Acharya, S.; Adamová, D.; Rinella, G. A.; **Chinellato, D. D. *; Guardiano, G. G.*; Liveraro, G. S. S.*; Takahashi, J.***; et al.
ALICE Collaboration

The first measurements of femtoscopic correlations with the particle pair combinations pi +/- K-S(0) in pp collisions at root s = 13 TeV at the Large Hadron Collider (LHC) are reported by the ALICE experiment. Using the femtoscopic approach, it is shown that it is possible to study the elusive K-0*(700) particle that has been considered a tetraquark candidate for over forty years. Source and final-state interaction parameters are extracted by fitting a model assuming a Gaussian source to the experimentally measured two-particle correlation functions. The final-state interaction in the pi +/- K-S(0) system is modeled through a resonant scattering amplitude, defined in terms of a mass and a coupling parameter, The extracted mass and Breit-Wigner width, derived from the coupling parameter, of the final-state interaction are found to be consistent with previous measurements of the K-0*(700). The small value and increase of the correlation strength with increasing source size support the hypothesis that the K-0*(700) is a four-quark state, i.e. a tetraquark state of the form (q(1), (q(2)) over bar, q(3), (q(3)) over bar) in which q(1), q(2) and q(3) indicate the flavor of the valence quarks of the pi and K-S(0). This latter trend is also confirmed via a simple geometric model that assumes a tetraquark structure of the K-0*(700) resonance.

PHYSICS LETTERS B 856, 138915, 2024. DOI: 10.1016/j.physletb.2024.138915

[P348-2024] "Isostructural Oxamate Complexes with Visible Luminescence (Eu3+) and Field-Induced Single-Molecule Magnet (Nd3+)"

Diogo, E. B. T.; da Silva Júnior, E. N.; Oliveira, W. X. C.; Stumpf, H. O.; **Fabris, F.*; de Almeida, A. A.*; Knobel, M.***; Ferreira, F. F.; Nunes, W. C.; Pedroso, E. F.; Julve, M.; Pereira, C. L. M.

The search for new metal-organic compounds as candidates for quantum information processing technologies is in the spotlight. Several metal ions and organic linkers have been used to obtain such compounds. Herein, we describe the synthesis, crystal structures, and cryomagnetic properties of two air-stable isostructural neodymium(III) and europium(III) one-dimensional (1D) coordination polymers of formula [Nd(Hmpa)(3)(DMSO)(2)](n) (1) and [Eu(Hmpa)(3)(DMSO)(2)](n) (2) [Hmpa=N-(4-methylphenyl)oxamate, and DMSO=dimethylsulfoxide]. These complexes were prepared by reacting n-Bu4N(Hmpa) proligand [n-Bu4N+=tetra-n-butylammonium] and the correspondent LnCl(3)center dot 6H(2)O salt (Ln=Nd or Eu) in the open air and mild conditions. The crystal structures of 1 and 2 reveal the Ln(3+) ion surrounded by two DMSO molecules and three oxamate ligands, one of them connecting to adjacent mononuclear entities through carboxylate bridges featuring a homometallic chain, while the other two establishing double N-H center dot center dot center dot O hydrogen bonds among adjacent polymers to give a resultant supramolecular 2D network. Cryomagnetic measurements in the static (dc) and dynamic current (ac) regimes reveal that 1 behaves as a field-induced single-molecule magnet below 8.8 K. A photoluminescence study shows that Hmpa ligands efficiently sensitize the luminescence of Eu3+ complex in the visible region in the solid state at room temperature.

CHEMISTRY-AN ASIAN JOURNAL 19[24], e202400887, 2024. DOI: 10.1002/asia.202400887

[P349-2024] "KS0 and Λ((Λ)over-bar) two-particle femtoscopic correlations in PbPb collisions at √sNN=5.02 TeV"

Tumasyan, A.; Adam, W.; Andrejkovic, J. W.; **Chinellato, J. A.*;** et al.
CMS Collaboration

Two-particle correlations are presented for K-S(0), Lambda, and (Lambda) over bar strange hadrons as a function of relative momentum in lead-lead collisions at a nucleon-nucleon center-of-mass energy of 5.02 TeV. The dataset corresponds to an integrated luminosity of 0.607 nb(-1) and was collected using the CMS detector at the CERN LHC. These correlations are sensitive to quantum statistics and to final-state interactions between the particles. The source size extracted from the (KSKS0)-K-0 correlations is found to decrease from 4.6 to 1.6 fm in going from central to peripheral collisions. Strong interaction scattering parameters (i.e., scattering length and effective range) are determined from the Lambda K-S(0) and Lambda Lambda (including their charge conjugates) correlations using the Lednicky-Lyuboshitz model and are compared to theoretical and other experimental results.

PHYSICS LETTERS B 857, 138936, 2024. DOI: 10.1016/j.physletb.2024.138936

[P350-2024] "Large-scale Cosmic-ray Anisotropies with 19 yr of Data from the Pierre Auger Observatory"

Halim, A. A.; Abreu, P.; Aglietta, M.; **Arbeletche, L. B.*; Chinellato, J. A.*; Dobrigkeit, C.*; Fauth, A. C.*; Payeras, A. M.*; Akim, J. V. R.*;** et al.
Pierre Auger Collaboration

Results are presented for the measurement of large-scale anisotropies in the arrival directions of ultra-high-energy cosmic rays detected at the Pierre Auger Observatory during 19 yr of operation, prior to AugerPrime, the upgrade of the observatory. The 3D dipole amplitude and direction are reconstructed above 4 EeV in four energy bins. Besides the established dipolar anisotropy in R.A. above 8 EeV, the Fourier amplitude of the 8-16 EeV energy bin is now also above the 5s discovery level.

No time variation of the dipole moment above 8 EeV is found, setting an upper limit to the rate of change of such variations of 0.3% yr(-1) at the 95% confidence level. Additionally, the results for the angular power spectrum are shown, demonstrating no other statistically significant multipoles. The results for the equatorial dipole component down to 0.03 EeV are presented, using for the first time a data set obtained with a trigger that has been optimized for lower energies. Finally, model predictions are discussed and compared with observations, based on two source emission scenarios obtained in the combined fit of spectrum and composition above 0.6 EeV.

ASTROPHYSICAL JOURNAL 976[1], 48, 2024. DOI: 10.3847/1538-4357/ad843b

[P351-2024] "Material extrusion of topologically engineered architecture inspired by carbon-based interlocked petal--schwarzites"

Ambekar, R. S.; Bastos, L.; **Galvao, D. S.***; Tiwary, C. S.; Woellner, C. F.

Exploiting the topologically engineered complex Schwarzite architecture has allowed the creation of innovative and distinctive structural elements possessing high specific strength. These fundamental building blocks' mechanical characteristics can be fine-tuned by reinforcing them with more robust architectures featuring high surface areas. In this work, we have fabricated six distinct Schwarzite-based structures composed of multiple interlocked layers, termed architecturally interlocked petal-schwarzites. These intricate structures have been additively manufactured into macroscopic dimensions and subjected to uniaxial compression. Experimental findings reveal a correlation between the mechanical response and the number of layers. Additionally, fully atomistic molecular dynamics compressive simulations have been carried out, yielding results that are in good agreement with the experimental observations. These simulations provide insights into the underlying mechanism of high specific strength and energy absorption exhibited by architecturally interlocked petal-schwarzites. The proposed methodology introduces a new perspective on the development of engineered additively manufactured materials with tunable and enhanced mechanical properties.

CARBON TRENDS 17, 100431, 2024. DOI: 10.1016/j.cartre.2024.100431

[P352-2024] "Measurement of (anti)alpha production in central Pb-Pb collisions at √sNN=5.02 TeV"

Acharya, S.; Adamová, D.; Rinella, G. A.; **Chinellato, D. D.*; Guardiano, G. G.*; Liveraro, G. S. S.*; Takahashi, J.***; et al.
ALICE Collaboration

In this letter, measurements of (anti)alpha production in central (0-10%) Pb-Pb collisions at a center-of-mass energy per nucleon-nucleon pair of root s(NN) = 5.02 TeV are presented, including the first measurement of an antialpha transverse-momentum spectrum. Owing to its large mass, the production of (anti)alpha is expected to be sensitive to different particle production models. The production yields and transverse-momentum spectra of nuclei are of particular interest because they provide a stringent test of these models. The averaged antialpha and alpha spectrum is compared to the spectra of lighter particles, by including it into a common blast-wave fit capturing the hydrodynamic-like flow of all particles. This fit is indicating that the (anti)alpha also participates in the collective expansion of the medium created in the collision. A blast-wave fit including only protons, (anti)alpha, and other light nuclei results in a similar flow velocity as the fit that includes all particles. A similar flow velocity, but a significantly larger kinetic freeze--out temperature is obtained when only protons and light nuclei are included in the fit. The coalescence parameter B-4 is well described by calculations from a statistical hadronization model but significantly underestimated by calculations assuming nucleus formation via coalescence of nucleons. Similarly, the (anti)alpha-to-proton ratio is well described by the statistical hadronization model. On the other hand, coalescence calculations including approaches with different implementations of the (anti)alpha substructure tend to underestimate the data.

PHYSICS LETTERS B 858, 138943, 2024. DOI: 10.1016/j.physletb.2024.138943

[P353-2024] "Measurement of beauty-quark production in pp collisions at √s=13 TeV via non-prompt D mesons"

Acharya, S.; Adamová, D.; Agarwal, A.; Rinella, G. A.; **Chinellato, D. D.*; Guardiano, G. G.*; Liveraro, G. S. S.*; Takahashi, J.***; et al.
ALICE Collaboration

The p(T)-differential production cross sections of non-prompt D-0, D+, and D+ s mesons originating from beauty-hadron decays are measured in proton-proton collisions at a centre-of--mass energy root s = 13TeV. The measurements are performed at midrapidity, |y| < 0.5, with the data sample collected by ALICE from 2016 to 2018. The results are in agreement with predictions from several perturbative QCD calculations. The fragmentation fraction of beauty quarks to strange mesons divided by the one to non-strange mesons, f(s)/(f(u)+ f(d)), is found to be 0.114 +/- 0.016 (stat.) +/- 0.006 (syst.) +/- 0.003 (BR) +/- 0.003 (extrap.). This value is compatible with previous measurements at lower centre-of-mass energies and in different collision systems in agreement with the assumption of universality of fragmentation functions. In addition, the dependence of the non-prompt D meson production on the centre-of-mass energy is investigated by comparing the results obtained at root s = 5.02 and 13TeV, showing a hardening of the non-prompt D-meson pT-differential production cross section at higher vs. Finally, the bb production cross section per unit of rapidity at midrapidity is calculated from the non-prompt D-0, D+, D-s(+), and Lambda(+)(c) hadron measurements, obtaining d sigma/dy = 75.2 +/- 3.2 (stat.) +/- 5.2 (syst.)(-3.2)(+12.3) (extrap.) mu b.

JOURNAL OF HIGH ENERGY PHYSICS [10], 110, 2024. DOI: 10.1007/JHEP10(2024)110

[P354-2024] "Measurement of boosted Higgs bosons produced via vector boson fusion or gluon fusion in the H -- b(b) over-bar decay mode using LHC proton-proton collision data at √s=13 TeV"

Hayrapetyan, A.; Tumasyan, A.; **Chinellato, J. A.***; et al.
CMS Collaboration

A measurement is performed of Higgs bosons produced with high transverse momentum (p(T)) via vector boson or gluon fusion in proton-proton collisions. The result is based on a data set with a center-of-mass energy of 13 TeV collected in 2016-2018 with the CMS detector at the LHC and corresponds to an integrated luminosity of 138 fb(-1). The decay of a high-p(T) Higgs boson to a boosted bottom quark-antiquark pair is selected using large-radius jets and employing jet substructure and heavy-flavor taggers based on machine learning techniques. Independent regions targeting the vector boson and gluon fusion mechanisms are defined based on the topology of two quark-initiated jets with large pseudorapidity separation. The signal strengths for both processes are extracted simultaneously by performing a maximum likelihood fit to data in the large-radius jet mass distribution.

The observed signal strengths relative to the standard model expectation are 4.9(-1.6)(+1.9) and 1.6(-1.5)(+1.7) for the vector boson and gluon fusion mechanisms, respectively. A differential cross section measurement is also reported in the simplified template cross section framework.

JOURNAL OF HIGH ENERGY PHYSICS [12], 035, 2024. DOI: 10.1007/JHEP12(2024)035

[P355-2024] "Measurement of Energy Correlators inside Jets and Determination of the Strong Coupling αS(mZ)"

Hayrapetyan, A.; Tumasyan, A.; Adam, W.; **Chinellato, J. A.***; et al.
CMS Collaboration

Energy correlators that describe energy-weighted distances between two or three particles in a hadronic jet are measured using an event sample of root s = 13 TeV proton-proton collisions collected by the CMS experiment and corresponding to an integrated luminosity of 36.3 fb(-1). The measured distributions are consistent with the trends in the simulation that reveal two key features of the strong interaction: confinement and asymptotic freedom. By comparing the ratio of the measured three- and two-particle energy correlator distributions with theoretical calculations that resum collinear emissions at approximate next-to-next-to-leading-logarithmic accuracy matched to a next-to-leading-order calculation, the strong coupling is determined at the Z boson mass: alpha(S)(m(Z)) = 0.1229(-0.0050)(+0.0040), the most precise alpha(S)(m(Z)) value obtained using jet substructure observables.

PHYSICAL REVIEW LETTERS 133[7], 071903, 2024. DOI: 10.1103/PhysRevLett.133.071903

[P356-2024] "Measurement of the Bs0 -- J/ψKS0 effective lifetime from proton-proton collisions at √s=13 TeV"

Hayrapetyan, A.; Tumasyan, A.; Adam, W.; **Chinellato, J. A.***; et al.
CMS Collaboration

The effective lifetime of the B-s(0) meson in the decay B-s(0) -> J/psi K-S(0) is measured using data collected during 2016-2018 with the CMS detector in root s = 13 TeV proton--proton collisions at the LHC, corresponding to an integrated luminosity of 140 fb(-1). The effective lifetime is determined by performing a two-dimensional unbinned maximum likelihood fit to the B-s(0) meson invariant mass and proper decay time distributions. The resulting value of 1.59 +/- 0.07(stat) +/- 0.03(syst) ps is the most precise measurement to date and is in good agreement with the expected value.

JOURNAL OF HIGH ENERGY PHYSICS 10, 247, 2024. DOI: 10.1007/JHEP10(2024)247

[P357-2024] "Measurement of the Higgs boson production via vector boson fusion and its decay into bottom quarks in proton-proton collisions at √s=13 TeV"

Hayrapetyan, A.; Tumasyan, A.; Adam, W.; Chinellato, J. A.*; et al.
CMS Collaboration

A measurement of the Higgs boson (H) production via vector boson fusion (VBF) and its decay into a bottom quark-antiquark pair (b (b) over bar) is presented using proton-proton collision data recorded by the CMS experiment at root s = 13 TeV and corresponding to an integrated luminosity of 90.8 fb(-1). Treating the gluon-gluon fusion process as a background and constraining its rate to the value expected in the standard model (SM) within uncertainties, the signal strength of the VBF process, defined as the ratio of the observed signal rate to that predicted by the SM, is measured to be mu(qqH)(Hb (b) over bar)=1.01(-0.46)(+0.55). The VBF signal is observed with a significance of 2.4 standard deviations relative to the background prediction, while the expected significance is 2.7 standard deviations. Considering inclusive Higgs boson production and decay into bottom quarks, the signal strength is measured to be mu(incl.)(Hbb) = 0.99(-0.41)(+0.48), corresponding to an observed (expected) significance of 2.6 (2.9) standard deviations.

JOURNAL OF HIGH ENERGY PHYSICS [1], 173, 2024. DOI: 10.1007/JHEP01(2024)173

[P358-2024] "Measurement of the impact-parameter dependent azimuthal anisotropy in coherent ρ0 photoproduction in Pb-Pb collisions at √sNN=5.02 TeV"

Acharya, S.; Adamová, D.; Agarwal, A.; Chinellato, D. D.*; Guardiano, G. G.*; Liveraro, G. S. S.*; Takahashi, J.*; et al.
ALICE Collaboration

This Letter presents the first measurement of the impact-parameter dependent angular anisotropy in the decay of coherently photoproduced rho(0) mesons. The rho(0) mesons are reconstructed through their decay into pion pairs. The measured anisotropy corresponds to the amplitude of the cos(2 phi) modulation, where phi is the angle between the two vectors formed by the sum and the difference of the transverse momenta of the pions, respectively. The measurement was performed by the ALICE Collaboration at the LHC using data from ultra-peripheral Pb-Pb collisions at a center-of-mass energy of root s(NN) = 5.02 TeV per nucleon pair. Different impact-parameter regions are selected by classifying the events in nuclear-breakup classes. The amplitude of the cos(2 phi) modulation is found to increase by about one order of magnitude from large to small impact parameters. Theoretical calculations describe the measured cos(2 phi) anisotropy and its impact-parameter dependence as the result of a quantum interference effect at the femtometer scale, arising from the ambiguity regarding which of the nuclei is the photon source in the interaction.

PHYSICS LETTERS B 858, 139017, 2024. DOI: 10.1016/j.physletb.2024.139017

[P359-2024] "Measurement of the polarizations of prompt and non-prompt J/ψ and ψ(2S) mesons produced in pp collisions at √s=13 TeV"

Hayrapetyan, A.; Tumasyan, A.; Adam, W.; **Chinellato, J. A.***; et al.
CMS Collaboration

The polarizations of prompt and non-prompt J/psi and psi(2S) mesons are measured in proton-proton collisions at root s = 13TeV, using data samples collected by the CMS experiment in 2017 and 2018, corresponding to a total integrated luminosity of 103.3 fb(-1). Based on the analysis of the dimuon decay angular distributions in the helicity frame, the polar anisotropy, lambda(theta), is measured as a function of the transverse momentum, p(T), of the charmonium states, in the 25-120 and 20-100GeV ranges for the J/psi and psi(2S), respectively. The non-prompt polarizations agree with predictions based on the hypothesis that, for p(T) greater than or similar to 25 GeV, the non-prompt J/psi and psi(2S) are predominantly produced in two-body B meson decays. The prompt results clearly exclude strong transverse polarizations, even for p(T) exceeding 30 times the J/psi mass, where lambda(theta) tends to an asymptotic value around 0.3. Taken together with previous measurements, by CMS and LHCb at root s = 7TeV, the prompt polarizations show a significant variation with p(T), at low p(T).

PHYSICS LETTERS B 858, 139044, 2024. DOI: 10.1016/j.physletb.2024.139044

[P360-2024] "Measurement of the production and elliptic flow of (anti)nuclei in Xe-Xe collisions at √sNN=5.44 TeV"

Acharya, S.; Adamová, D.; **Agarwal, A.*; Chinellato, D. D.*; Guardiano, G. G.*; Liveraro, G. S. S.*; Takahashi, J.*;** et al.
ALICE Collaboration

Measurements of (anti)deuteron and (anti)He-3 production in the rapidity range |y| < 0.5 as a function of the transverse momentum and event multiplicity in Xe-Xe collisions at a center--of-mass energy per nucleon-nucleon pair of root s(NN) = 5.44 TeV are presented. The coalescence parameters B-2 and B-3 are measured as a function of the transverse momentum per nucleon. The ratios between (anti)deuteron and (anti)He-3 yields and those of (anti)protons and pions are reported as a function of the mean charged-particle multiplicity density and compared with two implementations of the statistical hadronization model and with coalescence predictions. The elliptic flow of (anti)deuterons is measured for the first time in Xe-Xe collisions and shows features similar to those already observed in Pb-Pb collisions, i.e., the mass ordering at low transverse momentum and the meson-baryon grouping at intermediate transverse momentum. The production of nuclei is particularly sensitive to the chemical freeze-out temperature of the system created in the collision, which is extracted from a grandcanonical-ensemble-based thermal fit, performed for the first time including light nuclei along with light-flavor hadrons in Xe-Xe collisions. The extracted chemical freeze-out temperature T-chem = (154.2 +/- 1.1) MeV in Xe-Xe collisions is similar to that observed in Pb-Pb collisions and close to the crossover temperature predicted by lattice quantum chromodynamics calculations.

PHYSICAL REVIEW C 110[6], 064901, 2024. DOI: 10.1103/PhysRevC.110.064901

[P361-2024] "Measurement of the production cross section for a W boson in association with a charm quark in proton--proton collisions at √s=13 TeV"

Tumasyan, A.; Adam, W.; Andrejkovic, J. W.; **Chinellato, J. A.***; et al.
CMS Collaboration

The strange quark content of the proton is probed through the measurement of the production cross section for a W boson and a charm (c) quark in proton-proton collisions at a center--of-mass energy of 13 TeV. The analysis uses a data sample corresponding to a total integrated luminosity of 138 fb(-1) collected with the CMS detector at the LHC. The W bosons are identified through their leptonic decays to an electron or a muon, and a neutrino. Charm jets are tagged using the presence of a muon or a secondary vertex inside the jet. The W + c production cross section and the cross section ratio R-c(+/-) = sigma(W+ + (c) over bar)/sigma(W- + c) are measured inclusively and differentially as functions of the transverse momentum and the pseudorapidity of the lepton originating from the W boson decay. The precision of the measurements is improved with respect to previous studies, reaching 1% in R-c(+/-) = 0.950 +/- 0.005 (stat)+/- 0.010 (syst). The measurements are compared with theoretical predictions up to next-to-next--to-leading order in perturbative quantum chromodynamics.

EUROPEAN PHYSICAL JOURNAL C 84[1], 27, 2024. DOI: 10.1140/epjc/s10052-023-12258-4

[P362-2024] "Measurement of the production cross section of a Higgs boson with large transverse momentum in its decays to a pair of τ leptons in proton-proton collisions at √s=13 TeV"

Hayrapetyan, A.; Tumasyan, A.; Adam, W.; **Chinellato, J. A.***; et al.
CMS Collaboration

A measurement of the production cross section of a Higgs boson with transverse momentum greater than 250 GeV is presented where the Higgs boson decays to a pair of tau leptons. It is based on proton-proton collision data collected by the CMS experiment at the CERN LHC at a center-of-mass energy of 13 TeV. The data sample corresponds to an integrated luminosity of 138 fb(-1). Because of the large transverse momentum of the Higgs boson the tau leptons from its decays are boosted and produced spatially close, with their decay products overlapping. Therefore, a dedicated algorithm was developed to reconstruct and identify them. The observed (expected) significance of the measured signal with respect to the standard model background-only hypothesis is 3.5 (2.2) standard deviations. The product of the production cross section and branching fraction is measured to be 1.64(-0.54) (+0.68) times the standard model expectation. The fiducial differential production cross section is also measured as functions of the Higgs boson and leading jet transverse momenta. This measurement extends the probed large-transverse--momentum region in the tau tau final state beyond 600 GeV.

PHYSICS LETTERS B 857, 138964, 2024. DOI: 10.1016/j.physletb.2024.138964

[P363-2024] "Measurement of the τ lepton polarization in Z boson decays in proton-proton collisions at √s=13 TeV"

Hayrapetyan, A.; Tumasyan, A.; Adam, W.; **Chinellato, J. A.***; et al.
CMS Collaboration

The polarization of tau leptons is measured using leptonic and hadronic tau lepton decays in Z -> tau(+) tau(-) events in proton-proton collisions at root s = 13TeV recorded by CMS at the CERN LHC with an integrated luminosity of 36.3 fb(-1). The measured tau(-) lepton polarization at the Z boson mass pole is P-t(Z) = -0.144 +/- 0.006 (stat) +/- 0.014 (syst) = -0.144 +/- 0.015, in good agreement with the measurement of the tau lepton asymmetry parameter of A(tau) = 0.1439 +/- 0.0043 = -P-tau(Z) at LEP. The tau lepton polarization depends on the ratio of the vector to axial-vector couplings of the tau leptons in the neutral current expression, and thus on the effective weak mixing angle sin(2) theta(eff)(W), independently of the Z boson production mechanism. The obtained value sin(2) theta(eff)(W) = 0.2319 +/- 0.0008(stat) +/- 0.0018(syst) = 0.2319 +/- 0.0019 is in good agreement with measurements at e(+) e(-) colliders.

JOURNAL OF HIGH ENERGY PHYSICS [1], 101, 2024. DOI: 10.1007/JHEP01(2024)101

[P364-2024] "Measurement of Ωc0 baryon production and branching-fraction ratio BR(Ωc0 -- Ω-e+ve)/BR(Ωc0 -- Ω-π+) in pp collisions at √s=13 TeV"

Acharya, S.; Adamová, D.; Agarwal, A.; **Chinellato, D. D.*; Guardiano, G. G.*; Liveraro, G. S. S.*; Takahashi, J.***; et al.
ALICE Collaboration

The inclusive production of the charm-strange baryon Omega(0)(c) is measured for the first time via its semileptonic decay into Omega(-)e(+)nu(e) at midrapidity (vertical bar y vertical bar < 0.8) in proton-proton (pp) collisions at the center-of-mass energy root s =13 TeV with the ALICE detector at the LHC.

The transverse momentum (pT) differential cross section multiplied by the branching ratio is presented in the interval 2 < p(T) < 12 GeV=c. The branching-fraction ratio BR(Omega(0)(c) -> Omega(-)e(+)nu(e))/BR(Omega(0)(c) -> Omega(-)pi(+)) is measured to be 1.12 +/- 0.22 (stat) +/- 0.27 (syst). Comparisons with other experimental measurements, as well as with theoretical calculations, are presented.

PHYSICAL REVIEW D 110[3], 032014, 2024. DOI: 10.1103/PhysRevD.110.032014

[P365-2024] "Measurements of long-range two-particle correlation over a wide pseudorapidity range in p-Pb collisions at √sNN=5.02 TeV"

Acharya, S.; Adamová, D.; Rinella, G. A.; **Chinellato, D. D.*; Guardiano, G. G.*; Liveraro, G. S. S.*; Takahashi, J.*;** et al.
ALICE Collaboration

Correlations in azimuthal angle extending over a long range in pseudorapidity between particles, usually called the "ridge" phenomenon, were discovered in heavy-ion collisions, and later found in pp and p-Pb collisions. In large systems, they are thought to arise from the expansion (collective flow) of the produced particles. Extending these measurements over a wider range in pseudorapidity and final-state particle multiplicity is important to understand better the origin of these long-range correlations in small collision systems. In this Letter, measurements of the long-range correlations in p-Pb collisions at root s(NN) = 5.02TeV are extended to a pseudorapidity gap of Delta eta similar to 8 between particles using the ALICE forward multiplicity detectors. After suppressing non-flow correlations, e.g., from jet and resonance decays, the ridge structure is observed to persist up to a very large gap of Delta eta similar to 8 for the first time in p-Pb collisions. This shows that the collective flow-like correlations extend over an extensive pseudorapidity range also in small collision systems such as p-Pb collisions. The pseudorapidity dependence of the second-order anisotropic flow coefficient, v(2)(eta), is extracted from the long-range correlations. The v(2)(eta) results are presented for a wide pseudorapidity range of -3.1 < eta < 4.8 in various centrality classes in p-Pb collisions. To gain a comprehensive understanding of the source of anisotropic flow in small collision systems, the v(2)(eta) measurements are compared with hydrodynamic and transport model calculations. The comparison suggests that the final-state interactions play a dominant role in developing the anisotropic flow in small collision systems.

JOURNAL OF HIGH ENERGY PHYSICS [1], 199, 2024. DOI: 10.1007/JHEP01(2024)199

[P366-2024] "Measurements of polarization and spin correlation and observation of entanglement in top quark pairs using lepton plus jets events from proton-proton collisions at √s=13 TeV"

Hayrapetyan, A.; Tumasyan, A.; Adam, W.; **Chinellato, J. A.***; et al.
CMS Collaboration

Measurements of the polarization and spin correlation in top quark pairs (t (t) over bar) are presented using events with a single electron or muon and jets in the final state. The measurements are based on proton-proton collision data from the LHC at root s = 13 TeV collected by the CMS experiment, corresponding to an integrated luminosity of 138 fb(-1). All coefficients of the polarization vectors and the spin correlation matrix are extracted simultaneously by performing a binned likelihood fit to the data. The measurement is performed inclusively and in bins of additional observables, such as the mass of the t (t) over bar system and the top quark scattering angle in the t (t) over bar rest frame. The measured polarization and spin correlation are in agreement with the standard model. From the measured spin correlation, conclusions on the t (t) over bar spin entanglement are drawn by applying the Peres-Horodecki criterion. The standard model predicts entangled spins for t (t) over bar states at the production threshold and at high masses of the t (t) over bar system. Entanglement is observed for the first time in events at high t (t) over bar mass, where a large fraction of the t (t) over tilde decays are spacelike separated, with an expected and observed significance of above 5 standard deviations.

PHYSICAL REVIEW D 110[11], 112016, 2024. DOI: 10.1103/PhysRevD.110.112016

[P367-2024] "Multiplicity dependence of charged-particle intra-jet properties in pp collisions at √s=13 TeV"

Acharya, S.; Adamová, D.; Rinella, G. A.; **Chinellato, D. D.*; Guardiano, G. G.*; Liveraro, G. S. S.*; Takahashi, J.*;** et al.
ALICE Collaboration

The first measurement of the multiplicity dependence of intra-jet properties of leading charged-particle jets in proton--proton (pp) collisions is reported. The mean charged-particle multiplicity and jet fragmentation distributions are measured in minimum-bias and high-multiplicity pp collisions at center--of-mass energy root s = 13 TeV using the ALICE detector. Jets are reconstructed from charged particles produced in the midrapidity region (|eta| < 0.9) using the sequential recombination anti-kT algorithm with jet resolution parameters R = 0.2, 0.3, and 0.4 for the transverse momentum (p(T)) interval 5-110 GeV/c. The high-multiplicity events are selected by the forward V0 scintillator detectors. The mean charged-particle multiplicity inside the leading jet cone rises monotonically with increasing jet pT in qualitative agreement with previous measurements at lower energies. The distributions of jet fragmentation function variables z(ch) and xi(ch) are measured for different jet- pT intervals. Jet- pT independent fragmentation of leading jets is observed for wider jets except at high- and low-z(ch) values. The observed "hump-backed plateau" structure in the. ch distribution indicates suppression of low- p(T) particles. In high-multiplicity events, an enhancement of the fragmentation probability of low-zch particles accompanied by a suppression of high-z(ch) particles is observed compared to minimum-bias events. This behavior becomes more prominent for low- p(T) jets with larger jet radius. The results are compared with predictions of QCD-inspired event generators, PYTHIA8 with Monash 2013 tune and EPOS LHC. It is found that PYTHIA8 qualitatively reproduces the jet modification in high-multiplicity events except at high jet p(T). These measurements provide important constraints to models of jet fragmentation.

EUROPEAN PHYSICAL JOURNAL C 84[10], 1079, 2024. DOI: 10.1140/epjc/s10052-024-13228-0

[P368-2024] "Neutrino charge radius and additional one-loop radiative corrections at ultranear reactor experiments"

Brdar, V.; **Leite, L. J. F.***; Parker, G. A; Xu, X. J.

We scrutinize the potential of upcoming ultranear reactor neutrino experiments to detect radiative corrections in the elastic neutrino-electron scattering channel, focusing on the JUNO--TAO and CLOUD detectors, which employ advanced scintillator detection technologies. Previous reactor experiments have already constrained the electron neutrino charge radius, which is a neutrino property associated with a certain subset of the total radiative corrections, and have achieved limits that are only about an order of magnitude away from the Standard Model prediction. Our study demonstrates that JUNO-TAO and CLOUD could discover the neutrino charge radius in the near future, considering the established treatment of the charge radius.

However, we show that it is necessary to go beyond this standard treatment. By including the complete set of one-loop level radiative corrections, we find a partial cancellation with the charge radius effect, reducing the experimental sensitivity to this quantity. Nevertheless, JUNO-TAO and CLOUD still have the potential to achieve a 5 sigma discovery but over longer timescales within a reasonable operational time frame.

PHYSICAL REVIEW D 110[11], 113005, 2024. DOI: 10.1103/PhysRevD.110.113005

[P369-2024] "Observation of double J/ψ meson production in pPb collisions at √sNN=8.16 TeV"

Hayrapetyan, A.; Tumasyan, A; Adam, W.; **Chinellato, J. A.***; et al.
CMS Collaboration

The first observation of the concurrent production of two J/psi mesons in proton-nucleus collisions is presented. The analysis is based on a proton-lead (pPb) data sample recorded at a nucleon-nucleon center-of-mass energy of 8.16 TeV by the CMS experiment at the CERN LHC and corresponding to an integrated luminosity of 174.6 nb(-1). The two J/psi mesons are reconstructed in their mu(+)mu(-) decay channels with transverse momenta p(T) > 6.5 GeV and rapidity vertical bar y vertical bar < 2.4. Events where one of the J/psi mesons is reconstructed in the dielectron channel are also considered in the search. The pPb -> J/psi J/psi +X process is observed with a significance of 5.3 standard deviations. The measured inclusive fiducial cross section, using the four-muon channel alone, is sigma(pPb (-> J/psi J/psi + X) = 22.0 +/- 8.9(stat) +/- 1.5(syst) nb. A fit of the data to the expected rapidity separation for pairs of J/psi mesons produced in single (SPS) and double (DPS) parton scatterings yields sigma(pPb)(SPS) (-> J/psi J/psi + X) = 16.5 +/- 10.8(stat) +/- 0.1(syst) nb and sigma(pPb) (DPS) (-> J/psi J/psi + X) = 5.4 +/- 6.2(stat) +/- 0.4(syst) nb, respectively. This latter result can he transformed into a lower hound on the effective DPS cross section, closely related to the squared average interparton transverse separation in the collision, of sigma(eff) > 1.0 mb at 95% confidence level.

PHYSICAL REVIEW D 110[9], 092002, 2024. DOI: 10.1103/PhysRevD.110.092002

[P370-2024] "Observation of Enhanced Long-Range Elliptic Anisotropies Inside High-Multiplicity Jets in pp Collisions at √s=13 TeV"

Hayrapetyan, A.; Tumasyan, A.; Adam, W.; **Chinellato, J. A.***; et al.
CMS Collaboration

A search for collective effects inside jets produced in proton--proton collisions is performed via correlation measurements of charged particles using the CMS detector at the CERN LHC. The analysis uses data collected at a center-of-mass energy of root s = 13 TeV, corresponding to an integrated luminosity of 138 fb(-1). Jets are reconstructed with the anti-kT algorithm with a distance parameter of 0.8 and are required to have transverse momentum greater than 550 GeV and pseudorapidity vertical bar eta(jet)vertical bar < 1.6. Two-particle correlations among the charged particles within the jets are studied as functions of the particles' azimuthal angle and pseudorapidity separations (Delta phi* and Delta eta*) in a jet coordinate basis, where particles' eta*, phi* are defined relative to the direction of the jet. The correlation functions are studied in classes of in-jet chargedparticle multiplicity up to N-ch(J) approximate to 100. Fourier harmonics are extracted from long-range azimuthal correlation functions to characterize azimuthal anisotropy for vertical bar Delta eta*vertical bar > 2. For low-N--ch(j) jets, the long-range elliptic anisotropic harmonic, v(2)*, is observed to decrease with N-ch(j). This trend is well described by Monte Carlo event generators. However, a rising trend for v(2)* emerges at N-ch(j) greater than or similar to 80, hinting at a possible onset of collective behavior, which is not reproduced by the models tested. This observation yields new insights into the dynamics of jet evolution in the vacuum.

PHYSICAL REVIEW LETTERS 133[14], 142301, 2024. DOI: 10.1103/PhysRevLett.133.142301

[P371-2024] "Observation of Medium-Induced Yield Enhancement and Acoplanarity Broadening of Low-pT Jets from Measurements in pp and Central Pb-Pb Collisions at √sNN=5.02 TeV"

Acharya, S.; Adamová, D.; Rinella, G. A.; **Chinellato, D. D.*; Guardiano, G. G.*; Liveraro, G. S. S.*; Takahashi, J.*;** et al.
ALICE Collaboration

The ALICE Collaboration reports the measurement of semi--inclusive distributions of charged-particle jets recoiling from a high transverse momentum (high p(T)) hadron trigger in proton-proton and central Pb-Pb collisions at root S-NN = 5.02 TeV. A data-driven statistical method is used to mitigate the large uncorrelated background in central Pb-Pb collisions. Recoil jet distributions are reported for jet resolution parameter R = 0.2, 0.4, and 0.5 in the range 7 < p(T, jet) < 140 GeV/c and trigger--recoil jet azimuthal separation pi/2 < Delta phi < pi. The measurements exhibit a marked medium-induced jet yield enhancement at low pT and at large azimuthal deviation from Delta phi similar to pi. The enhancement is characterized by its dependence on Delta phi, which has a slope that differs from zero by 4.7 sigma. Comparisons to model calculations incorporating different formulations of jet quenching are reported. These comparisons indicate that the observed yield enhancement arises from the response of the QGP medium to jet propagation.

PHYSICAL REVIEW LETTERS 133[2], 022301, 2024. DOI: 10.1103/PhysRevLett.133.022301

[P372-2024] "Observation of quantum entanglement in top quark pair production in proton-proton collisions at √s=13 TeV"

Hayrapetyan, A.; Tumasyan, A.; Adam, W.; **Chinellato, J. A.***; et al.
CMS Collaboration

Entanglement is an intrinsic property of quantum mechanics and is predicted to be exhibited in the particles produced at the Large Hadron Collider. A measurement of the extent of entanglement in top quark-antiquark (t (t) over bar) events produced in proton-proton collisions at a center-of-mass energy of 13 TeV is performed with the data recorded by the CMS experiment at the CERN LHC in 2016, and corresponding to an integrated luminosity of 36.3 fb(-1). The events are selected based on the presence of two leptons with opposite charges and high transverse momentum. An entanglement-sensitive observable D is derived from the top quark spin-dependent parts of the t (t) over bar production density matrix and measured in the region of the t (t) over bar production threshold. Values of D < -1/3 are evidence of entanglement and D is observed (expected) to be -0.480(-0.029)(+0.026) (-0.467(-0.029)(+0.026)) at the parton level. With an observed significance of 5.1 standard deviations with respect to the non-entangled hypothesis, this provides observation of quantum mechanical entanglement within t (t) over bar pairs in this phase space. This measurement provides a new probe of quantum mechanics at the highest energies ever produced.

REPORTS ON PROGRESS IN PHYSICS 87[11], 117801, 2024. DOI: 10.1088/1361-6633/ad7e4d

[P373-2024] "Performance of CMS muon reconstruction from proton-proton to heavy ion collisions"

Hayrapetyan, A.; Tumasyan, A.; Adam, W.; **Chinellato, J. A.***; et al.
CMS Collaboration

The performance of muon tracking, identification, triggering, momentum resolution, and momentum scale has been studied with the CMS detector at the LHC using data collected at root s(NN) = 5.02 TeV in proton-proton (pp) and lead-lead (PbPb) collisions in 2017 and 2018, respectively, and at root s(NN) = 8.16 TeV in proton-lead (pPb) collisions in 2016. Muon efficiencies, momentum resolutions, and momentum scales are compared by focusing on how the muon reconstruction performance varies from relatively small occupancy pp collisions to the larger occupancies of pPb collisions and, finally, to the highest track multiplicity PbPb collisions. We find the efficiencies of muon tracking, identification, and triggering to be above 90% throughout most of the track multiplicity range. The momentum resolution and scale are unaffected by the detector occupancy. The excellent muon reconstruction of the CMS detector enables precision studies across all available collision systems.

JOURNAL OF INSTRUMENTATION 19[9], P09012, 2024. DOI: 10.1088/1748-0221/19/09/P09012

[P374-2024] "Performance of the CMS electromagnetic calorimeter in pp collisions at √s=13 TeV"

Hayrapetyan, A.; Tumasyan, A.; Adam, W.; **Chinellato, J. A.***; et al.
CMS Collaboration

The operation and performance of the Compact Muon Solenoid (CMS) electromagnetic calorimeter (ECAL) are presented, based on data collected in pp collisions at root s = 13 TeV at the CERN LHC, in the years from 2015 to 2018 (LHC Run 2), corresponding to an integrated luminosity of 151 fb(-1). The CMS ECAL is a scintillating lead-tungstate crystal calorimeter, with a silicon strip preshower detector in the forward region that provides precise measurements of the energy and the time-of-arrival of electrons and photons. The successful operation of the ECAL is crucial for a broad range of physics goals, ranging from observing the Higgs boson and measuring its properties, to other standard model measurements and searches for new phenomena. Precise calibration, alignment, and monitoring of the ECAL response are important ingredients to achieve these goals. To face the challenges posed by the higher luminosity, which characterized the operation of the LHC in Run 2, the procedures established during the 2011-2012 run of the LHC have been revisited and new methods have been developed for the energy measurement and for the ECAL calibration. The energy resolution of the calorimeter, for electrons from Z boson decays reaching the ECAL without significant loss of energy by bremsstrahlung, was better than 1.8%, 3.0%, and 4.5% in the vertical bar eta vertical bar intervals [0.0, 0.8], [0.8, 1.5], [1.5, 2.5], respectively. This resulting performance is similar to that achieved during Run 1 in 2011-2012, in spite of the more severe running conditions.

JOURNAL OF INSTRUMENTATION 19[9], P09004, 2024. DOI: 10.1088/1748-0221/19/09/P09004

[P375-2024] "Performance of the CMS high-level trigger during LHC Run 2"

Hayrapetyan, A.; Tumasyan, A.; Adam, W.; **Chinellato, J. A.***; et al.
CMS Collaboration

The CERN LHC provided proton and heavy ion collisions during its Run 2 operation period from 2015 to 2018. Proton-proton collisions reached a peak instantaneous luminosity of 2.1 x 10(34) cm(-2)s(-1), twice the initial design value, at root s = 13 TeV. The CMS experiment records a subset of the collisions for further processing as part of its online selection of data for physics analyses, using a two-level trigger system: the Level-1 trigger, implemented in custom-designed electronics, and the high-level trigger, a streamlined version of the offline reconstruction software running on a large computer farm. This paper presents the performance of the CMS high-level trigger system during LHC Run 2 for physics objects, such as leptons, jets, and missing transverse momentum, which meet the broad needs of the CMS physics program and the challenge of the evolving LHC and detector conditions. Sophisticated algorithms that were originally used in offline reconstruction were deployed online. Highlights include a machine-learning b tagging algorithm and a reconstruction algorithm for tau leptons that decay hadronically.

JOURNAL OF INSTRUMENTATION 19[11], P11021, 2024. DOI: 10.1088/1748-0221/19/11/P11021

[P376-2024] "Pulse Dynamics in Reduced Graphene Oxide Electrolyte-Gated Transistors: Charge Memory Effects and Mechanisms Governing the Ion-To-Electron Transduction"

Selmi, G. S.; Neto, E. R. L.; Lelis, G. C; Okazaki, A. K.; **Riul Jr, A.*; Braunger, M. L.* Oliveira, R. F.***

Electrolyte-gated transistors (EGTs) are widely employed in bioelectronics due to their ability to bridge ionic and electronic phenomena in a single device. Among potential materials, reduced graphene oxide (rGO) has gained significant attention due to its ambipolar current response, quantum capacitance, and tunable conductivity. However, the rGO EGT dynamic behavior remains significantly unexplored. Here, the time-dependent response of rGO EGTs is systematically investigated under gate voltage pulsing across different time scales (10 ms to 40 s) and amplitudes (up to |+/- 0.8 V|). Significant charge memory is observed, particularly for long (40 s) pulses at 0.8 V, with effects also evident for shorter (1 s) and weaker stimuli (0.6 V). Multiple low-level (0.1 V) fast pulsing (100 ms) further demonstrate charge retention post-stimulation. All these characteristics are attributed to a complex interplay between ion entrapment within the rGO film, electrical double-layer formation, and charge transfer processes. The stability of rGO EGTs under prolonged bias stress is also examined, aiming to contribute to the development of more robust devices. These findings revealed the complex role of electrolyte ions and electronic carriers governing the ion-to-electron transduction and charge memory effects in rGO EGTs, contributing to the advancement of the next-generation bioelectronic devices.

ADVANCED ELECTRONIC MATERIALS, 2024. DOI: 10.1002/aelm.202400791 Early Access Date: DEC 2024

[P377-2024] "Robust single-photon generation for quantum information enabled by stimulated adiabatic rapid passage"

Karli, Y.; Schwarz, R.; Kappe, F.; Vajner, D. A.; Krämer, R. G.; **Silva, S. F. C.***

The generation of single photons using solid-state quantum emitters is pivotal for advancing photonic quantum technologies, particularly in quantum communication. As the field continuously advances toward practical use cases and beyond shielded laboratory environments, specific demands are placed on the robustness of quantum light sources during operation. In this context, the robustness of the quantum light generation process against intrinsic and extrinsic effects is a major challenge. Here, we present a robust scheme for the coherent generation of indistinguishable single-photon states with very low photon

number coherence using a three-level system in a semiconductor quantum dot. Our approach combines the advantages of adiabatic rapid passage and stimulated two-photon excitation. We demonstrate robust quantum light generation while maintaining the prime quantum-optical quality of the emitted light state. Moreover, we highlight the immediate advantages of the implementation of various quantum cryptographic protocols.

APPLIED PHYSICS LETTERS 125[25], 254002, 2024. DOI: 10.1063/5.0241504

[P378-2024] "Search for a resonance decaying to a W boson and a photon in proton-proton collisions at √s=13 TeV using leptonic W boson decays"

Hayrapetyan, A.; Tumasyan, A.; Adam, W.; **Chinellato, J. A.***; et al.
CMS Collaboration

A search for a new charged particle X with mass between 0.3 and 2.0TeV decaying to a W boson and a photon is presented, using proton-proton collision data at a center-of-mass energy of 13TeV, collected by the CMS experiment and corresponding to an integrated luminosity of 138 fb(-1). Particle X has electric charge +/- 1 and is assumed to have spin 0. The search is performed using the electron and muon decays of the W boson. No significant excess above the predicted background is observed. The upper limit at 95% confidence level on the product of the production cross section of the X and its branching fraction to a W boson and a photon is found to be 94 (137) fb for a 0.3TeV resonance and 0.75 (0.81) fb for a 2.0TeV resonance, for an X width-to-mass ratio of 0.01% (5%). This search presents the most stringent constraints to date on the existence of such resonances across the probed mass range. A statistical combination with an earlier study based on the hadronic decay mode of the W boson is also performed, and the upper limit at 95% confidence level for a 2.0TeV resonance is reduced to 0.50 (0.63) fb for an X width-to-mass ratio of 0.01% (5%).

JOURNAL OF HIGH ENERGY PHYSICS [9], 186, 2024. DOI: 10.1007/JHEP09(2024)186

[P379-2024] "Search for a scalar or pseudoscalar dilepton resonance produced in association with a massive vector boson or top quark-antiquark pair in multilepton events at √s=13 TeV"

Tumasyan, A.; Adam, W.; Andrejkovic, J. W.; **Chinellato, J. A.***; et al.
CMS Collaboration

A search for beyond the standard model spin-0 bosons, phi, that decay into pairs of electrons, muons, or tau leptons is presented. The search targets the associated production of such bosons with a W or Z gauge boson, or a top quark-antiquark pair, and uses events with three or four charged leptons, including hadronically decaying tau leptons. The proton-proton collision data set used in the analysis was collected at the LHC from 2016 to 2018 at a center-of-mass energy of 13 TeV, and corresponds to an integrated luminosity of 138 fb(-1). The observations are consistent with the predictions from standard model processes. Upper limits are placed on the product of cross sections and branching fractions of such new particles over the mass range of 15 to 350 GeV with scalar, pseudoscalar, or Higgs-boson-like couplings, as well as on the product of coupling parameters and branching fractions. Several model-dependent exclusion limits are also presented. For a Higgs-boson-like phi model, limits are set on the mixing angle of the Higgs boson with the phi boson. For the associated production of a phi boson with a top quark--antiquark pair, limits are set on the coupling to top quarks. Finally, limits are set for the first time on a fermiophilic dilaton-like model with scalar couplings and a fermiophilic axion-like model with pseudoscalar couplings.

PHYSICAL REVIEW D 110[1], 012013, 2024. DOI: 10.1103/PhysRevD.110.012013

[P380-2024] "Search for an exotic decay of the Higgs boson into a Z boson and a pseudoscalar particle in proton-proton collisions at √s=13TeV"

Hayrapetyan, A.; Tumasyan, A.; Adam, W.; **Chinellato, J. A.***; et al.
CMS Collaboration

A search for an exotic decay of the Higgs boson to a Z boson and a light pseudoscalar particle (a), decaying to a pair of leptons and a pair of photons, respectively, is presented. The search is based on proton-proton collision data at a center-of-mass energy of root s = 13 TeV, collected with the CMS detector at the LHC and corresponding to an integrated luminosity of 138 fb(-1). The analysis probes pseudoscalar masses m(a) between 1 and 30 GeV, leading to two pairs of well-isolated leptons and photons. Upper limits at 95% confidence level are set on the Higgs boson production cross section times its branching fraction to two leptons and two photons. The observed (expected) limits are in the range of 1.1-17.8 (1.7-17.9) f(b) within the probed m(a) interval. An excess of data above the expected standard model background with a local (global) significance of 2.6 (1.3) standard deviations is observed for a mass hypothesis of m(a) = 3 GeV. Limits on models involving axion-like particles, formulated as an effective field theory, are also reported.

PHYSICS LETTERS B 852,138582, 2024. DOI: 10.1016/j.physletb.2024.138582

[P381-2024] "Search for bottom-type vectorlike quark pair production in dileptonic and fully hadronic final states in proton-proton collisions at √s=13 TeV"

Hayrapetyan, A.; Tumasyan, A.; Adam, W.; **Chinellato, J. A.*;** et al.
CMS Collaboration

A search is described for the production of a pair of bottom--type vectorlike quarks (B VLQs) with mass greater than 1000 GeV. Each B VLQ decays into a b quark and a Higgs boson, a b quark and a Z boson, or a t quark and a W boson. This analysis considers both fully hadronic final states and those containing a charged lepton pair from a Z boson decay. The products of the H -> bb boson decay and of the hadronic Z or W boson decays can be resolved as two distinct jets or merged into a single jet, so the final states are classified by the number of reconstructed jets. The analysis uses data corresponding to an integrated luminosity of 138 fb(-1) collected in proton--proton collisions at root s = 13 TeV with the CMS detector at the LHC from 2016 to 2018. No excess over the expected background is observed. Lower limits are set on the B VLQ mass at the 95% confidence level. These depend on the B VLQ branching fractions and are 1570 and 1540 GeV for 100% B -> bH and 100% B -> bZ, respectively. In most cases, the mass limits obtained exceed previous limits by at least 100 GeV.

PHYSICAL REVIEW D 110[5], 052004, 2024. DOI: 10.1103/PhysRevD.110.052004

[P382-2024] "Search for Higgs boson pair production in the b(b)over-bar W+W- decay mode in proton-proton collisions at √s=13 TeV"

Hayrapetyan, A.; Tumasyan, A.; Adam, W.; **Chinellato, J. A.***; et al.
CMS Collaboration

A search for Higgs boson pair (HH) production with one Higgs boson decaying to two bottom quarks and the other to two W bosons are presented. The search is done using proton-proton collisions data at a centre-of-mass energy of 13TeV, corresponding to an integrated luminosity of 138 fb(-1) recorded by the CMS detector at the LHC from 2016 to 2018. The final states considered include at least one leptonically decaying W boson. No evidence for the presence of a signal is observed and corresponding upper limits on the HH production cross section are derived. The limit on the inclusive cross section of the nonresonant HH production, assuming that the distributions of kinematic observables are as expected in the standard model (SM), is observed (expected) to be 14 (18) times the value predicted by the SM, at 95% confidence level. The limits on the cross section are also presented as functions of various Higgs boson coupling modifiers, and anomalous Higgs boson coupling scenarios. In addition, limits are set on the resonant HH production via spin-0 and spin-2 resonances within the mass range 250-900 GeV.

JOURNAL OF HIGH ENERGY PHYSICS [7], 293, 2024. DOI: 10.1007/JHEP07(2024)293

[P383-2024] "Search for long-lived particles decaying in the CMS muon detectors in proton-proton collisions at √s=13 TeV"

Hayrapetyan, A.; Tumasyan, A.; Adam, W.; **Chinellato, J. A.***; et al.
CMS Collaboration

A search for long-lived particles (LLPs) decaying in the CMS muon detectors is presented. A data sample of proton-proton collisions at root s = 13 TeV corresponding to an integrated luminosity of 138 fb(-1), recorded at the LHC in 2016-2018, is used. The decays of LLPs are reconstructed as high multiplicity clusters of hits in the muon detectors. In the context of twin Higgs models, the search is sensitive to LLP masses from 0.4 to 55 GeV and a broad range of LLP decay modes, including decays to hadrons, tau leptons, electrons, or photons. No excess of events above the standard model background is observed. The most stringent limits to date from LHC data are set on the branching fraction of the Higgs boson decay to a pair of LLPs with masses below 10 GeV. This search also provides the best limits for various intervals of LLP proper decay length and mass. Finally, this search sets the first limits at the LHC on a dark quantum chromodynamic sector whose particles couple to the Higgs boson through gluon, Higgs boson, photon, vector, and dark-photon portals, and is sensitive to branching fractions of the Higgs boson to dark quarks as low as 2 x 10(-3).

PHYSICAL REVIEW D 110[3], 032007, 2024. DOI: 10.1103/PhysRevD.110.032007

[P384-2024] "Search for new physics in high-mass diphoton events from proton-proton collisions at √s=13 TeV"

Hayrapetyan, A.; Tumasyan, A.; Adam, W.; **Chinellato, J. A.***; et al.
CMS Collaboration

Results are presented from a search for new physics in high--mass diphoton events from proton-proton collisions at root s = 13TeV. The data set was collected in 2016-2018 with the CMS detector at the LHC and corresponds to an integrated luminosity of 138 fb(-1). Events with a diphoton invariant mass greater than 500 GeV are considered. Two different techniques are used to predict the standard model backgrounds: parametric fits to the smoothly-falling background and a first-principles calculation of the standard model diphoton spectrum at next-to-next-to-leading order in perturbative quantum chromodynamics calculations. The first technique is sensitive to resonant excesses while the second technique can identify broad differences in the invariant mass shape. The data are used to constrain the production of heavy Higgs bosons, Randall-Sundrum gravitons, the large extra dimensions model of Arkani-Hamed, Dimopoulos, and Dvali (ADD), and the continuum clockwork mechanism. No statistically significant excess is observed. The present results are the strongest limits to date on ADD extra dimensions and RS gravitons with a coupling parameter greater than 0.1.

JOURNAL OF HIGH ENERGY PHYSICS [8], 215, 2024. DOI: 10.1007/JHEP08(2024)215

[P385-2024] "Search for photons above 1018 eV by simultaneously measuring the atmospheric depth and the muon content of air showers at the Pierre Auger Observatory"

Halim, A. A.; Abreu, P.; Aglietta, M.; **Bonneau A. L.*; Chinellato, J. A.*; Dobrigkeit, C.*; Fauth, A. C.*; Machado Payeras, A.*; Reginatto Akim, J. V.*;** et al.
Pierre Auger Collaboration

The Pierre Auger Observatory is the most sensitive instrument to detect photons with energies above 1017 eV. It measures extensive air showers generated by ultrahigh energy cosmic rays using a hybrid technique that exploits the combination of a fluorescence detector with a ground array of particle detectors. The signatures of a photon-induced air shower are a larger atmospheric depth of the shower maximum (X-max) and a steeper lateral distribution function, along with a lower number of muons with respect to the bulk of hadron-induced cascades. In this work, a new analysis technique in the energy interval between 1 and 30 EeV (1 EeV = 10(18) eV) has been developed by combining the fluorescence detector-based measurement of Xmax with the specific features of the surface detector signal through a parameter related to the air shower muon content, derived from the universality of the air shower development. No evidence of a statistically significant signal due to photon primaries was found using data collected in about 12 years of operation. Thus, upper bounds to the integral photon flux have been set using a detailed calculation of the detector exposure, in combination with a data-driven background estimation. The derived 95% confidence level upper limits are 0.0403, 0.01113, 0.0035, 0.0023, and 0.0021 km(-2) sr(-1) yr(-1) above 1, 2, 3, 5, and 10 EeV, respectively, leading to the most stringent upper limits on the photon flux in the EeV range. Compared with past results, the upper limits were improved by about 40% for the lowest energy threshold and by a factor 3 above 3 EeV, where no candidates were found and the expected background is negligible. The presented limits can be used to probe the assumptions on chemical composition of ultrahigh energy cosmic rays and allow for the constraint of the mass and lifetime phase space of super-heavy dark matter particles.

PHYSICAL REVIEW D 110[6], 062005, 2024. DOI: 10.1103/PhysRevD.110.062005

[P386-2024] "Search for production of a single vectorlike quark decaying to tH or tZ in the all-hadronic final state in pp collisions at √s=13 TeV"

Hayrapetyan, A.; Tumasyan, A.; Adam, W.; **Chinellato, J. A.***; et al.
CMS Collaboration

A search for electroweak production of a single vectorlike T quark in association with a bottom (b) quark in the all-hadronic decay channel is presented. This search uses proton-proton collision data at root s = 13 TeV

collected by the CMS experiment at the CERN LHC during 2016-2018, corresponding to an integrated luminosity of 138 fb(-1). The T quark is assumed to have charge 2/3 and decay to a top (t) quark and a Higgs (H) or Z boson. Hadronic decays of the t quark and the H or Z boson are reconstructed from the kinematic properties of jets, including those containing b hadrons. No deviation from the standard model prediction is observed in the reconstructed tH and tZ invariant mass distributions. The 95% confidence level upper limits on the product of the production cross section and branching fraction of a T quark produced in association with a b quark and decaying via tH or tZ range from 1260 to 68 fb for T quark masses of 600-1200 GeV.

PHYSICAL REVIEW D 110[7], 072012, 2024. DOI: 10.1103/PhysRevD.110.072012

[P387-2024] "Search for Soft Unclustered Energy Patterns in Proton-Proton Collisions at 13 TeV"

Hayrapetyan, A.; Tumasyan, A.; Adam, W.; **Chinellato, J. A.***; et al.
CMS Collaboration

The first search for soft unclustered energy patterns (SUEPs) is performed using an integrated luminosity of 138 fb(-1) of proton-proton collision data at root s = 13 TeV, collected in 2016-2018 by the CMS detector at the LHC. Such SUEPs are predicted by hidden valley models with a new, confining force with a large't Hooft coupling. In events with boosted topologies, selected by high-threshold hadronic triggers, the multiplicity and sphericity of clustered tracks are used to reject the background from standard model quantum chromodynamics. With no observed excess of events over the standard model expectation, limits are set on the cross section for production via gluon fusion of a scalar mediator with SUEP-like decays.

PHYSICAL REVIEW LETTERS 133[19], 191902, 2024. DOI: 10.1103/PhysRevLett.133.191902

[P388-2024] "Search for the Z Boson Decay to ττμμ in Proton-Proton Collisions at √s=13 TeV"

Hayrapetyan, A.; Tumasyan, A.; Adam, W.; **Chinellato, J. A.***; et al.
CMS Collaboration

The first search for the Z boson decay to tau tau mu mu at the CERN LHC is presented, based on data collected by the CMS experiment at the LHC in proton-proton collisions at a center-of-mass energy of 13 TeV and corresponding to an integrated luminosity of 138 fb(-1). The data are compatible with the predicted background. For the first time, an upper limit at the 95% confidence level of 6.9 times the standard model expectation is placed on the ratio of the Z -> tau tau mu mu to Z -> 4 mu branching fractions. Limits are also placed on the six flavor-conserving four-lepton effective-field-theory operators involving two muons and two tau leptons, for the first time testing all such operators.

PHYSICAL REVIEW LETTERS 133[16], 161805, 2024. DOI: 10.1103/PhysRevLett.133.161805

[P389-2024] "Searches for Pair-Produced Multijet Resonances Using Data Scouting in Proton-Proton Collisions at √s=13 TeV"

Hayrapetyan, A.; Tumasyan, A.; Kodolova, O.; **Chinellato, J. A.***; et al.
CMS Collaboration

Searches for pair-produced multijet signatures using data corresponding to an integrated luminosity of 128 fb(-1) of proton-proton collisions at root s = 13 TeV are presented. A data scouting technique is employed to record events with low jet scalar transverse momentum sum values. The electroweak production of particles predicted in R-parity violating supersymmetric models is probed for the first time with fully hadronic final states. This is the first search for prompt hadronically decaying mass-degenerate higgsinos, and extends current exclusions on R-parity violating top squarks and gluinos.

PHYSICAL REVIEW LETTERS 133[20], 201803, 2024. DOI: 10.1103/PhysRevLett.133.201803

[P390-2024] "Searches for violation of Lorentz invariance in top quark pair production using dilepton events in 13 TeV proton-proton collisions"

Hayrapetyan, A.; Tumasyan, A.; Adam, W.; **Chinellato, J. A.***; et al.
CMS Collaboration

A search for violation of Lorentz invariance in the production of top quark pairs (t (t) over bar) is presented. The measured normalized differential t (t) over bar production cross section, as a function of the sidereal time, is examined for potential modulations induced by Lorentz-invariance breaking operators in an effective field theory extension of the standard model (SM). The cross section is measured from collision events collected by the CMS detector at a center-of-mass-energy of 13 TeV, corresponding to an integrated luminosity of 77.8 fb(-1), and containing one electron and one muon. The results are found to be compatible with zero, in agreement with the SM, and are used to place upper limits at 68% confidence level on the magnitude of the Lorentz-violating couplings ranging from 1-8 x 10(-3). This is the first precision test of the isotropy in special relativity with top quarks at the LHC, restricting further the bounds on such couplings by up to two orders of magnitude with respect to previous searches conducted at the Tevatron.

PHYSICS LETTERS B 857, 138979, 2024. DOI: 10.1016/j.physletb.2024.138979

[P391-2024] "SPT clusters with DES and HST weak lensing. I. Cluster lensing and Bayesian population modeling of multiwavelength cluster datasets"

Bocquet, S.; Grandis, S.; Bleem, L. E.; **Navarro-Alsina, A.*;** et al.
DES Collaboration; SPT Collaboration

We present a Bayesian population modeling method to analyze the abundance of galaxy clusters identified by the South Pole Telescope (SPT) with a simultaneous mass calibration using weak gravitational lensing data from the Dark Energy Survey (DES) and the Hubble Space Telescope (HST). We discuss and validate the modeling choices with a particular focus on a robust, weak-lensing-based mass calibration using DES data. For the DES Year 3 data, we report a systematic uncertainty in weak-lensing mass calibration that increases from 1% at z = 0.25 to 10% at z = 0.95, to which we add 2% in quadrature to account for uncertainties in the impact of baryonic effects. We implement an analysis pipeline that joins the cluster abundance likelihood with a multiobservable likelihood for the Sunyaev-Zel'dovich effect, optical richness, and weak-lensing measurements for each individual cluster. We validate that our analysis pipeline can recover unbiased cosmological constraints by analyzing mocks that closely resemble the cluster sample extracted from the SPT-SZ, SPTpol ECS, and SPTpol 500d surveys and the DES Year 3 and HST-39 weak-lensing datasets. This work represents a crucial prerequisite for the subsequent cosmological analysis of the real dataset.

PHYSICAL REVIEW D 110[8], 083509, 2024. DOI: 10.1103/PhysRevD.110.083509

[P392-2024] "SPT clusters with DES and HST weak lensing. II. Cosmological constraints from the abundance of massive halos"

Bocquet, S.; Grandis, S.; Bleem, L. E.; **Navarro-Alsina, A.*;** et al.
SPT Collaboration; DES Collaboration

We present cosmological constraints from the abundance of galaxy clusters selected via the thermal Sunyaev-Zel'dovich (SZ) effect in South Pole Telescope (SPT) data with a simultaneous mass calibration using weak gravitational lensing data from the Dark Energy Survey (DES) and the Hubble Space Telescope (HST). The cluster sample is constructed from the combined SPT-SZ, SPTpol ECS, and SPTpol 500d surveys, and comprises 1,005 confirmed clusters in the redshift range 0.25-1.78 over a total sky area of 5200 deg(2). We use DES Year 3 weak-lensing data for 688 clusters with redshifts z < 0.95 and HST weaklensing data for 39 clusters with 0.6 < z < 1.7. The weak-lensing measurements enable robust mass measurements of sample clusters and allow us to empirically constrain the SZ observable-mass relation without having to make strong assumptions about, e.g., the hydrodynamical state of the clusters. For a flat.CDMcosmology, and marginalizing over the sum of massive neutrinos, we measure Omega(m) = 0.286 +/- 0.032, sigma(8) = 0.817 +/- 0.026, and the parameter combination sigma(8)(Omega(m)=0.3)(0.25) = 0.805 +/- 0.016. Our measurement of S-8 = sigma(8)root Omega(m)/0.3 = 0.795 +/- 0.029 and the constraint from Planck CMB anisotropies (2018 TT, TE, EE + lowE) differ by 1.1s. In combination with that Planck dataset, we place a 95% upper limit on the sum of neutrino masses Sigma m(nu) < 0.18 eV. When additionally allowing the dark energy equation of state parameter w to vary, we obtain w = -1.45 +/- 0.31 from our cluster--based analysis. In combination with Planck data, we measure w = - 1.34(-0.15)(+0.22), or a 2.2 sigma difference with a cosmological constant. We use the cluster abundance to measure sigma(8) in five redshift bins between 0.25 and 1.8, and we find the results to be consistent with structure growth as predicted by the Lambda CDM model fit to Planck primary CMB data.

PHYSICAL REVIEW D 110[8], 083510, 2024. DOI: 10.1103/PhysRevD.110.083510

[P393-2024] "Strong enhancement of effective refractive index in structured colloids (TiO2@Silica): Localization of light"

Dipold, J.; Wetter, N. U.; **Marques, F. C.***; Dogariu, A.; **Jiménez-Villar, E.***

We use non-resonant Raman scattering to demonstrate a large enhancement of the effective refractive index experienced by Raman photons in a scattering medium comprising spatially--correlated photonic structures of core-shell TiO2@Silica scatterers mixed with silica nanoparticles and suspended in ethanol. We show that the high refractive index extends outside the physical boundary of the medium, which is attributed to the evanescent contributions of electromagnetic modes that are strongly localized within the medium. Notably, the effective enhancement can be observed even at very low intensities of Raman emission. This anomalous non-linear phenomenon could be explained by the successive polarization of valence electrons to virtual states induced by the strong photon correlations in the strongly localized electromagnetic modes. The enhancement of refractive index and its extension in the vicinity of the medium's interface provide new opportunities for controlling the electromagnetic fields in advanced photonic devices.

NANOSCALE, 2024. DOI: 10.1039/d4nr03626c Early Access Date: DEC 2024

[P394-2024] "Study of charm hadronization with prompt Λc+ baryons in proton-proton and lead-lead collisions at √sNN=5.02 TeV"

Tumasyan, A.; Adam, W.; Andrejkovic, J. W.; **Chinellato, J. A.*; et al.**
CMS Collaboration

The production of prompt Lambda(+)(c) baryons is measured via the exclusive decay channel Lambda(+)(c) -> pK(-) pi(+) at a center-of-mass energy per nucleon pair of 5.02TeV, using proton-proton (pp) and lead-lead (PbPb) collision data collected by the CMS experiment at the CERN LHC. The pp and PbPb data were obtained in 2017 and 2018 with integrated luminosities of 252 and 0.607 nb(-1), respectively. The measurements are performed within the Lambda(+)(c) rapidity interval vertical bar y vertical bar < 1 with transverse momentum (p(T)) ranges of 3-30 and 6-40 GeV/c for pp and PbPb collisions, respectively. Compared to the yields in pp collisions scaled by the expected number of nucleon-nucleon interactions, the observed yields of Lambda(+)(c) with p(T) > 10 GeV/c are strongly suppressed in PbPb collisions. The level of suppression depends significantly on the collision centrality. The Lambda(+)(c)/D-0 production ratio is similar in PbPb and pp collisions at p(T) > 10 GeV/c, suggesting that the coalescence process does not play a dominant role in prompt Lambda(+)(c) baryon production at higher p(T).

JOURNAL OF HIGH ENERGY PHYSICS [1], 128, 2024. DOI: 10.1007/JHEP01(2024)128

[P395-2024] "Studying the interaction between charm and light-flavor mesons"

Acharya, S.; Adamová, D.; Rinella, G. A.; **Chinellato, D. D.*; Guardiano, G. G.*; Liveraro, G. S. S.*; Takahashi, J.*;** et al.
ALICE Collaboration

The two-particle momentum correlation functions between charm mesons (D*(+/-) and D-+/-) and charged light-flavor mesons (pi(+/-) and K-+/-) in all charge combinations are measured for the first time by the ALICE Collaboration in high-multiplicity proton-proton collisions at a center-of-mass energy of root S = 13 TeV. For DK and D*K pairs, the experimental results are in agreement with theoretical predictions of the residual strong interaction based on quantum chromodynamics calculations on the lattice and chiral effective field theory. In the case of D pi and D*pi pairs, tension between the calculations including strong interactions and the measurement is observed. For all particle pairs, the data can be adequately described by Coulomb interaction only, indicating a shallow interaction between charm and light-flavor mesons. Finally, the scattering lengths governing the residual strong interaction of the D pi and D*pi systems are determined by fitting the experimental correlation functions with a model that employs a Gaussian potential. The extracted values are small and compatible with zero.

PHYSICAL REVIEW D 110[3], 032004, 2024. DOI: 10.1103/PhysRevD.110.032004

[P396-2024] "Tau polarization effects in ν τ / ν τ- tungsten interactions at the LHC energies"

Francener, R.*; Gonçalves, V. P.; **Gratieri, D. R.*; Diego R.***

Recent studies have demonstrated that the tau produced in charged current neutrino deeply inelastic interactions at the GeV-TeV neutrino energy range is not fully polarized. In this paper we investigate the impact of the tau polarization on the pions generated in its decay. In particular, we consider tau neutrinotungsten interactions at the LHC energies and estimate the associated pion momentum, energy, and angular distributions.

The contribution of the F5 is also investigated. Our results indicate that the pion properties are sensitive to the tau polarization state as well as to the magnitude of F5.

PHYSICAL REVIEW D 110[7], 073006, 2024. DOI: 10.1103/PhysRevD.110.073006

[P397-2024] "The DUNE far detector vertical drift technology Technical design report"

Abud, A. Abed.; Abi, B.; Acciarri, R.; **Adriano, C.*; Bazetto, M. C. Q.*; Borges Merlo, R.*; De Aguiar, R.*; De Almeida, P.*; De Holanda, P. C.*; Gelli, B.*; Gratieri, D. R.*; Guzzo, M. M.*; Kemp, E.*; Machado, A. A.*; Das Chagas Marques, F.*; Peres, O. L. G.*; Pimentel, V. L.*; Segreto, E.*;** et al.
DUNE Collaboration

DUNE is an international experiment dedicated to addressing some of the questions at the forefront of particle physics and astrophysics, including the mystifying preponderance of matter over antimatter in the early universe. The dual-site experiment will employ an intense neutrino beam focused on a near and a far detector as it aims to determine the neutrino mass hierarchy and to make high-precision measurements of the PMNS matrix parameters, including the CP-violating phase. It will also stand ready to observe supernova neutrino bursts, and seeks to observe nucleon decay as a signature of a grand unified theory underlying the standard model. The DUNE far detector implements liquid argon time-projection chamber (LArTPC) technology, and combines the many tens-of-kiloton fiducial mass necessary for rare event searches with the sub-centimeter spatial resolution required to image those events with high precision. The addition of a photon detection system enhances physics capabilities for all DUNE physics drivers and opens prospects for further physics explorations. Given its size, the far detector will be implemented as a set of modules, with LArTPC designs that differ from one another as newer technologies arise. In the vertical drift LArTPC design, a horizontal cathode bisects the detector, creating two stacked drift volumes in which ionization charges drift towards anodes at either the top or bottom. The anodes are composed of perforated PCB layers with conductive strips, enabling reconstruction in 3D. Light-trap-style photon detection modules are placed both on the cryostat's side walls and on the central cathode where they are optically powered. This Technical Design Report describes in detail the technical implementations of each subsystem of this LArTPC that, together with the other far detector modules and the near detector, will enable DUNE to achieve its physics goals.

JOURNAL OF INSTRUMENTATION 19[8], T08004, 2024. DOI: 10.1088/1748-0221/19/08/T08004

[P398-2024] "Unruh-deWitt detector in impulsive plane wave spacetimes"

Pitelli, J. P. M.*; Mosna, R. A.*

We investigate the response function of an inertial Unruh--deWitt detector in an impulsive plane wave spacetime. Through symmetry considerations applied to the Wightman function, we demonstrate that the response function remains invariant for any inertial detector, even for those experiencing a discontinuous light cone coordinate shift after interacting with the shock wave. This implies that the vacuum state in an impulsive plane wave spacetime is preserved under the associated spacetime symmetries. Additionally, we confirm that the quantum imprint of the shock wave, as discussed in Gray et al. [J. High Energy Phys. 11 (2021) 054], is not an artifact and exhibits a distinct characteristic form. We identify this form by defining a "renormalized" response function for an eternally inertial detector, with Minkowski spacetime as a reference.

PHYSICAL REVIEW D 110[12], 125002, 2024. DOI: 10.1103/PhysRevD.110.125002

Artigos publicados 2025

[P001-2025] "A planar-sheet nongraphitic zero-bandgap sp2 carbon phase made by the low-temperature reaction of γ-graphyne"

Aliev, A. E.; Guo, Yongzhe; **Fonseca, A. F.***; Razal, J. M.; Wang, Z.; **Galvão, D. S.***; Bolding, C. M.; Chapman-Wilson, N. E.; Desyatkin, V. G.; Leisen, J. E.; Ribeiro Junior, L. A.; **Kanegae, G. B.*;** Lynch, P.; Zhang, J.; Judicpa, M. A.; Parra, A. M.; Zhang, M.; Gao, E.; Hu, L.; Rodionov, V. O.; Baughman, R. H.

The highest sheet symmetry form of graphyne, with one triple bond between each neighboring hexagon in graphene, irreversibly transforms exothermically at ambient pressure and low temperatures into a nongraphitic, planar-sheet, zero-bandgap phase consisting of intrasheet-bonded sp2 carbons. The synthesis of this sp2 carbon phase is demonstrated, and other carbon phases are described for possible future synthesis from graphyne without breaking graphyne bonds. While measurements and theory indicate that the reacting graphyne becomes nonplanar because of sheet wrinkling produced by dimensional mismatch between reacted and nonreacted sheet regions, sheet planarity is regained when the reaction is complete. Although the observed elimination of triple bonds to make parallel planar sp2 carbon sheets likely requires ordered transformation within each sheet, diffraction data for reacted multisheet stacks indicate that the relative lateral positions of neighboring sheets are disordered, as predicted, since no crystalline diffraction peak (other than for the intersheet spacing) is observed.

PROCEEDINGS OF THE NATIONAL ACADEMY OF SCIENCES OF THE UNITED STATES OF AMERICA 122[5], e2413194122, 2025. DOI: 10.1073/pnas.2413194122

[P002-2025] "Addressing γ5 in nondimensional regularizations: a case study on the Bumblebee model"

Rosado, R. J. C.; **Cherchiglia, A.***; Sampaio, M.; Hiller, B.

We examine the subtleties of regularization schemes in four-dimensional space (4S), related in particular to the introduction of the gamma 5 matrix. To illustrate we use a "Bumblebee" model featuring dynamically induced Lorentz symmetry violation. The analysis centers on how different regularization methods affect the solutions to the gap equation in this model. We highlight the resolution of ambiguities associated with the gamma 5 matrix in ultraviolet divergent integrals by employing an enhanced Implicit Regularization (IREG) method. This method extends IREG to a quasi-four-dimensional space, Q4S=4S circle plus X, drawing parallels with the consistent approach of Dimensional Reduction (DRED). Comparative analysis is conducted against results from the 't Hooft-Veltman regularization scheme, conventional IREG in strict 4S, and sharp momentum cutoff techniques. Our results illustrate a scheme to compute gamma 5 interactions in physical dimension of divergent amplitudes, confirming the approach in Bruque et al. (JHEP 08:109, 2018).

EUROPEAN PHYSICAL JOURNAL C 85[1], 41, 2025. DOI: 10.1140/epjc/s10052-025-13756-3

[P003-2025] "Angular dependence of four mechanical properties of graphynes"

Kanegae, G. B.*; Fonseca, A. F.*

Graphyne is a porous two-dimensional carbon allotrope of graphene that possesses interesting physical properties, including non-null bandgap. It is composed of carbon hexagonal rings or carbon-carbon bonds connected by acetylenic chains. The diverse forms of these connections yield a variety of graphyne structures. In a previous study, we have obtained the elastic properties of seven distinct families of graphyne structures as a function of the number of acetylene chains, from 1 to 10. The Young's modulus, shear modulus, Poisson's ratio and linear compressibility were predicted for the zigzag and armchair directions of all 70 graphyne structures. Here, we present some noteworthy findings regarding the angular dependence of these four elastic properties of asymmetric graphynes. Our results demonstrate that in a single structure, the minimum and maximum Young's modulus can vary by a factor of 10. Additionally, the directions of null linear compressibility in some asymmetric structures were determined.Graphical abstractAngular dependence of the mechanical properties of one asymmetric graphyne. Each quadrant shows one mechanical property. Each quadrant shows curves in the angular range of 90 degrees corresponding to different sizes of acetylene chains in the graphyne structure.

MRS ADVANCES, 2025. DOI: 10.1557/s43580-025-01124-y. Early Access Date: JAN 2025

[P004-2025] "Coverage- and temperature-induced self-metalation of tetraphenyltransdibenzoporphyrin on Cu(111)"

Shaker, M.; Muth, M.; Steffen, J.; **Santos, A. C. dos***; Jaekel, S.; Adhikari, R.; Gazetas, P.; Oleszak, C.; **Siervo, A. de***; Jux, N.; Görling, A.; Lytken, O.; Steinrück, H. P.

We have investigated the adsorption and self-metalation of free-base tetraphenyltransdibenzoporphyrin (2H-TPtdBP) on Cu(111) as a function of coverage and temperature using scanning tunneling microscopy, x-ray photoelectron spectroscopy, temperature programmed desorption, and density--functional theory calculations. At low coverages (<0.16 molecules nm(-2)), we observe isolated individual molecules with an inverted conformation and no self-metalation up to 363 K. At higher coverages, both the formation of ordered islands and self-metalation are observed over time already at room temperature, and accelerate upon heating to 363 K. At 423 K, complete self-metalation occurs for all coverages up to the completed first layer. By comparing our results for 2H-TPtdBP to the existing literature on other tetraphenyl--based porphyrins, we demonstrate how adsorption and self--metalation can be tailored by the choice of substituents.

JOURNAL OF PHYSICS-CONDENSED MATTER 37[8], 085001, 2025. DOI: 10.1088/1361-648X/ad92d2

[P005-2005] "Effects of annealing temperature on the formability, mechanical and interface properties of laminated metal composite STS304L/Al1050/STS430"

Pertile, F.; Ismail, S.; **Leidens, L. M.***; Schaeffer, L.; Figueroa, C. A.; Michels, A. F.

Laminated metallic composites (LMCs) produced by cold roll bonding generate high plastic deformation. After the rolling process, it is essential to promote a post-heat treatment (PHT) to increase adhesion, minimize hardening, and enhance the formability of LMCs. In this research, the effects of PHT at low temperatures (250, 350, and 450 degrees C) on LMCs (STS304/Al1050/STS430) obtained by cold rolling were investigated. The Forming Limit Curve (FLC) and mechanical properties such as ultimate tensile strength (sigma_UT), yield strength (sigma_Y), elongation (epsilon), and the anisotropy index (r-value) of the LMC were evaluated. Results indicate the best PHT temperature that combines formability, increased adhesion between layers, and better mechanical properties, such as elongation (epsilon), which increases from 37% to 55%. At this PHT temperature, the brittle intermetallic layer was not detected, and the FLC showed the best performance. Furthermore, in industrial applications, this PHT condition allows energy savings compared to PHT conditions of high process times (>12 h) and/or temperature (>500 degrees C) reported by several works in the literature.

JOURNAL OF COMPOSITE MATERIALS, 2025. DOI: 10.1177/00219983251314158. Early Access Date: JAN 2025

[P006-2025] "Electron Spin Resonance (ESR) studies on GdCuBi2 intermetallic antiferromagnet"

Freitas, G. S.*; Pizzi, H.*; Carneiro, F. B.; **Carvalho, M. H.***; Bittar, E. M.; Bauer, E. D.; Thompson, J. D.; Ronning, F.; Thomas, S. M.; Rosa, P. F. S.; Greer, S. M.; **Pagliuso, P. G.***

We report temperature dependent X-Band (nu approximate to 9.5 GHz) Electron Spin Resonance (ESR) on the GdCuBi2 intermetallic compound. This compound presents a metallic Curie-Weiss paramagnetic behavior at high temperatures and orders antiferromagnetically at T-N = 14.3 K. Well above T-N (T > 250 K), the ESR experiments revealed temperature independent g-values spectra composed of a single Dysonian Gd3+ ESR line for the studied compound. Within the same temperature range, the Gd3+ ESR linewidth Delta H presents a linear broadening temperature dependence known as Korringa behavior. The obtained Korringa rate (Delta H/Delta T) and g-shift (Delta g) from the ESR measurements, along with the study of the macroscopic properties of GdCuBi2 (e.g. specific heat data and magnetic susceptibility) made it possible to explore Gd3+ spin dynamics in this system based on evaluation of the exchange parameters between the Gd3+ ESR probes and the conduction-electrons (ce) in this compound. Our results indicate that the exchange bottleneck effects and a <bold>q</bold>-dependent exchange interaction (J(fs)(q)) between the Gd(3+)4f and the ce are likely to be present in GdCuBi2. Disregarding the bottleneck effects in the simplest approximation, we extract the exchange parameters J(fs)(q=0) approximate to 380 meV and <J(fs)(2)(q)>(1/2)approximate to 3.0 meV for the Gd3+ spin dynamics in GdCuBi2. These values of J(fs)(q) and <J(fs)(2)(q)>(1/2) are typical of Gd3+ local moments in intermetallic materials and the small ratio [<J(fs)(2)(q)>/J(fs)(2)(0)] approximate to 0.008 suggests a strongly anisotropic (or quasi-2D) Fermi surface for GdCuBi2.

JOURNAL OF MAGNETISM AND MAGNETIC MATERIALS 613, 172651, 2025. DOI: 10.1016/j.jmmm.2024.172651

[P007-2025] "Enhanced Non-Invasive Radio Frequency Heating Using 2D Pyrite (Pyritene)"

Rajeev, K.; **Ipaves, B.***; Oliveira, C. C. de; Raman, S. P.; Kar, S.; **Galvao, D. S.***; Autreto, P. A. da S.; Tiwary, C. S.

Radiofrequency (RF) heating is a new, less invasive alternative to invasive heating methods that use nanoparticles for tumour therapy. But pinpoint local heating is still hard. Molecular interactions form a hybrid structure with unique electrical characteristics that enable RF heating in this work, which explores RF heating in a biological cell (yeast)--2D FeS2 system. Substantial processes have been uncovered via experimental investigations and density functional theory (DFT) computations. At 3 W and 50 MHz, RF heating reaches 54 degrees C in 40 s, which is enough to kill yeast cells, while current-voltage measurements reveal ionic diode-like properties. Interactions between yeast lipid molecules and 2D FeSk, as shown by density-functional theory calculations,

cause an imbalance in the distribution of charges and the creation of polar, conductive channels. Insights into biological heating applications based on radio frequency (RF) technology are offered by this work, which lays forth a framework for investigating 2D material-biomolecule interactions.

SMALL METHODS, 2025. DOI: 10.1002/smtd.202402066. Early Access Date: FEB 2025

[P008-2025] "Enhanced performance of impedimetric immunosensors to detect SARS-CoV-2 with bare gold nanoparticles and graphene acetic acid"

Hensel, R. C.; Di Vizio, B.; Materòn, E. M.; **Shimizu, F. M.***; Angelim, M. K. S. C.; Souza, G. F.; Módena, J. L. P.; Moraes-Vieira, P. M. M.; Azevedo, R. B. de; Litti, L.; Agnoli, S.; Casalini, S.; Oliveira Jr., O. N.

Immunosensors based on electrical impedance spectroscopy allow for label-free, real-time detection of biologically relevant molecules and pathogens, without requiring electro-active materials. Here, we investigate the influence of bare gold nanoparticles (AuNPs), synthesized via laser ablation in solution, on the performance of an impedimetric immunosensor for detecting severe acute respiratory syndrome coronavirus (SARS-CoV-2). Graphene acetic acid (GAA) was used in the active layer for immobilizing anti-SARS-CoV-2 antibodies, owing to its high density of carboxylic groups. Immunosensors incorporating AuNPs exhibited superior performance compared to those relying solely on GAA, achieving a limit of detection (LoD) of 3 x 10-20 g/mL to detect the Spike Receptor Binding Domain (RBD) protein of SARS-CoV-2 and of 2 PFU/mL for inactivated virus. Moreover, these immunosensors presented high selectivity against the H1N1 influenza virus. We anticipate that this platform will be versatile and applicable in the early diagnosis of various diseases and viral infections, thereby facilitating Point-of-Care testing.

TALANTA 281, 126903, 2025. DOI: 10.1016/j.talanta.2024.126903

[P009-2025] "How does goldene stack?"

Pereira, Jr., M. L.; Santos, E. J. A. dos; Ribeiro Jr., L. A.; **Galvao, D. S.***

The recent synthesis of goldene, a 2D atomic monolayer of gold, has opened new avenues in exploring novel materials. However, the question of when multilayer goldene transitions into bulk gold remains unresolved. This study used density functional theory calculations to address this fundamental question. Our findings reveal that multilayer goldene retains an AA-like stacking configuration of up to six layers, with no observation of Bernal-like stacking as seen in graphene. Goldene spontaneously transitions to a bulk-like gold structure at seven layers, adopting a rhombohedral (ABC-like) stacking characteristic of bulk face-centered cubic (FCC) gold. The atomic arrangement converges entirely to the bulk gold lattice for more than ten layers. Quantum confinement significantly impacts the electronic properties, with monolayer and bulk goldene exhibiting levels with linear dispersion at the X-point of the Brillouin zone. In contrast, multilayer goldene shows levels with linear dispersions at the X- and Y-points. Monolayer goldene exhibits anisotropic optical absorption, which is absent in bulk gold. This study provides a deeper understanding of multilayer goldene's structural and electronic properties and stacked 2D materials in general.

MATERIALS HORIZONS, 2025. DOI: 10.1039/d4mh01319k. Early Access Date: JAN 2025

[P010-2025] "Identification and analysis of reference-independent movement event-related desynchronization"

Melo, G. C. de*; Castellano, G.*; Forner-Cordero, A.

Characterization of the electroencephalography (EEG) signals related to motor activity, such as alpha- and beta-band motor event-related desynchronizations (ERDs), is essential for Brain Computer Interface (BCI) development. Determining the best electrode combination to detect the ERD is crucial for the success of the BCI. Considering that the EEG signals are bipolar, this involves the choice of the main and reference electrodes. So far, no strategy to guarantee signals free of the activity from the reference electrode has achieved consensus among the scientific community. Therefore, mapping the ERD in terms of the spatial distribution of the main and reference electrodes can provide additional perspectives for the BCI field. The goal of this work is to identify subject-specific channels where ERD is temporally coupled to the initiation of an upper-limb motor task. We defined a criterion to determine the presence of the ERD linked to the movement onset and searched, separately for each subject, for the single channel with the most prominent ERD. The search was conducted over all available channels composed by a pair of electrodes, and the selected signals were analyzed according to their temporal and spatial characteristics. We found that alpha- and beta-band ERD temporarily linked to movement onset can be detected in atypical channels (pairs of electrodes) across the scalp. The selected channels were different across subjects. Four ERD temporal patterns were observed in terms of the initiation instant of the ERD. These patterns revealed that the M1 cortex seems to be related to later ERDs. Moreover, they were also associated to different cortical processes related to the motor task. To the best of our knowledge, this is the first time these findings are reported. Aiming at BCI development, further experiments with more subjects and with motor-imagery tasks are desirable for more robustness and applicability of these findings.

BIOMEDICAL PHYSICS & ENGINEERING EXPRESS 11[2], 025001, 2025. DOI: 10.1088/2057-1976/ada1dc

[P011-2025] "Investigating the impact of ITO substrates on the optical and electronic properties of WSe2 monolayers"

Brito, T. G. L.*; Costa, F. J. R.*; Ceccatto, A.*; Almeida, C. A. N. de*; Siervo, A. de*; Couto Jr., O. D. D.*; Barcelos, I. D.; **Zagonel, L. F.***

Two-dimensional (2D) materials, particularly transition metal dichalcogenides (TMDs), have gathered significant attention due to their interesting electrical and optical properties. Among TMDs, monolayers of WSe2 exhibit a direct band gap and high exciton binding energy, which enhances photon emission and absorption even at room temperature. This study investigates the electronic and optical properties of WSe2 monolayers when they are mechanically transferred to indium tin oxide (ITO) substrates. ITO is a transparent conducting electrode (TCE) used in many industrial optoelectronic applications. Samples were mechanically transferred under ambient conditions, consequently trapping an adsorbate layer of atmospheric molecules unintentionally between the monolayer and the substrate. To reduce the amount of adsorbates, some samples were thermally annealed. Atomic force microscopy confirmed the presence of the adsorbate layer under the TMD and its partial removal after annealing.X-ray photoelectron spectroscopy confirmed the presence of carbon species among the adsorbates even after annealing. Photoluminescence measurements show that WSe2 remains optically active on ITO even after annealing. Moreover, the luminescence intensity and energy are affected by the amount of adsorbates under the WSe2 monolayer. Scanning tunnelling spectroscopy reveals that the TMD monolayer is n-doped, and that its band edges form a type I band alignment with ITO. Surface potential measurements show a polarity change after annealing, indicating that polar molecules, most likely water, are being removed.

This comprehensive study shows that a TCE does not quench WSe2 luminescence even after a prolonged thermal annealing, although its optical and electronic properties are affected by unintentional adsorbates. These findings provide insights for better understanding, controlling, and design of 2D material heterostructures on TCEs.

NANOTECHNOLOGY 36[5], 055704, 2025. DOI: 10.1088/1361-6528/ad8fb4

[P012-2025] "Magnetic properties of the RNiIn4 (R = Ce, Pr, Nd) series of intermetallic compounds grown by the metallic flux method"

Possidonio, D. N.; **Caffer, A. M.***; Mercena, S. G.; Santos, W. O.; **Freitas, G. S.*; Pagliuso, P. G.*;** Jesus, C. B. R.

This work focuses on the synthesis, structural and magnetic characterization, and the effects of the Crystal Electric Field (CEF) of RNiIn4 (R = Ce, Pr, Nd) compounds. By using the metal flux technique, high-quality single crystals were obtained and analyzed X-ray diffraction and confirmed the formation of a single phase for all compounds and revealed their crystallization in a orthorhombic structure. Magnetic susceptibility measurements revealed antiferromagnetic in ordering temperatures (TN) at 4.02 K, 2.37 K and 4.06 for Ce, Pr, and Nd, respectively. Specific heat data corroborated these findings. The results indicate the easy axis of magnetization lies in the ab-plane for Ce and Nd, and along the c-axis for Pr.

JOURNAL OF MAGNETISM AND MAGNETIC MATERIALS 614, 172679, 2025. DOI: 10.1016/j.jmmm.2024.172679

[P013-2025] "Observation of Resistive Transitions in Copper Due to Proximity to a Frustrated Antiferromagnetic Insulator"

Pimentel, D. P.*

This work experimentally explores the induction of resistive transitions in a metal through the magnetic proximity effect, focusing specifically on the transitions in the electrical resistance of copper induced by the magnetic transitions of copper oxychloride. The findings unveiled a sharp drop in the electrical resistance of the conductive channel within the metallized regime, precisely coinciding with the magnetic transitions of copper oxychloride. The study's findings align with prior research on spin resistivity in frustrated antiferromagnet, and this phenomenon can be attributed to the induction of triplet states within the metallic layer via the magnetic proximity effect. These insights hold the potential to unlock new avenues for the investigation of spintronic devices and magnetic interface phenomena.

JOURNAL OF LOW TEMPERATURE PHYSICS, 2025. DOI: 10.1007/s10909-024-03260-5. Early Access Date: JAN 2025

[P014-2025] "Proximity-induced flipped spin state in synthetic ferrimagnetic Pt/Co/Gd heterolayers"

Brandao, J.; Carvalho, P. C.; Miranda, I. P.; Mori, T. J. A.; **Béron, F.*;** Bergman, A.; Petrilli, H. M.; Klautau, A. B.; Cezar, J. C.

To develop new devices based on synthetic ferrimagnetic heterostructures, understanding the material's physical properties is pivotal. Here, the induced magnetic moment (IMM), magnetic exchange coupling, and spin textures are investigated in Pt(1 nm)/Co(1.5 nm)/Gd(1 nm) multilayers using a multiscale approach. The magnitude and direction of the IMM are interpreted in the framework of both X-ray magnetic circular dichroism and density functional theory. The IMM transferred by Co across the Gd paramagnetic thickness leads to a nontrivial flipped spin state (FSS) within the Gd layers, in which their magnetic moments couple antiparallel/parallel with the ferromagnetic Co near/far from the Co/Gd interface, respectively. The FSS depends on the magnetic field, which, on average, reduces the Gd magnetic moment as the field increases. For the Pt, in both Pt/Co and Gd/Pt interfaces, the IMM follows the same direction as the Co magnetic moment, with negligible IMM in the Gd/Pt interface. Additionally, zero-field spin spirals were imaged using scanning transmission X-ray microscopy, whereas micromagnetic simulations were employed to unfold the interactions, stabilizing the ferrimagnetic configurations, where the existence of a sizable Dzyaloshinskii-Moriya interaction is demonstrated to be crucial.

COMMUNICATIONS PHYSICS 8[1], 22, 2025. DOI: 10.1038/s42005-025-01938-0

[P015-2025] "Rapidity dependence of antideuteron coalescence in pp collisions at √s=13 TeV with ALICE"

Acharya, S.; Adamova, D.; Agarwal, A.; **Chinellato, D. D.*; Guardiano, G. G.*; Liveraro, G. S. S.*; Takahashi, J.***; et al. ALICE Collaboration

The production yields of antideuterons and antiprotons are measured in pp collisions at a center-of-mass energy of root s = 13 TeV, as a function of transverse momentum (p(T)) and rapidity (y), for the first time rapidity-differentially up to vertical bar y vertical bar = 0.7. The measured spectra are used to study the p(T) and rapidity dependence of the coalescence parameter B-2, which quantifies the coalescence probability of antideuterons. The p(T) and rapidity dependence of the obtained B-2 is extrapolated for p(T) > 1.7 GeV/c and vertical bar y vertical bar > 0.7 using the phenomenological antideuteron production model implemented in PYTHIA 8.3 as well as a baryon coalescence afterburner model based on EPOS 3. Such measurements are of interest to the astrophysics community, since they can be used for the calculation of the flux of antinuclei from cosmic rays, in combination with coalescence models.

PHYSICS LETTERS B 860, 139191, 2025. DOI: 10.1016/j.physletb.2024.139191

[P016-2025] "Results from ON-OFF Analysis of the Neutrinos-Angra Detector"

Kemp, E.*; Santos, W. V. dos*; Anjos, J. C. dos; Chimenti, P.; Gonzalez, L. F. G.; Guedes, G. P.; Lima Jr, H. P.; Nóbrega, R. A.; Pepe, I. M.; Ribeiro, D. B. dos S.

The Neutrinos Angra Experiment, a water-based Cherenkov detector, is located at the Angra dos Reis nuclear power plant in Brazil. Designed to detect electron antineutrinos produced in the nuclear reactor, the primary objective of the experiment is to demonstrate the feasibility of monitoring reactor activity using an antineutrino detector. This effort aligns with the International Atomic Energy Agency (IAEA) program to identify potential and novel technologies applicable to nonproliferation safeguards. Operating on the surface presents challenges such as high noise rates, necessitating the development of very sensitive, yet small-scale detectors. These conditions make the Angra experiment an excellent platform for both developing the application and gaining expertise in new technologies and analysis methods. The detector employs a water-based target doped with gadolinium to enhance its sensitivity to antineutrinos. In this work, we describe the main features of the detector and the electronics chain, including front-end and data acquisition components. We detail the data acquisition strategies and the methodologies applied for signal processing and event selection.

Preliminary physics results suggest that the detector can reliably monitor reactor operations by detecting the inverse beta decay induced by electron antineutrinos from the reactor.

BRAZILIAN JOURNAL OF PHYSICS 55[1], 39, 2054. DOI: 10.1007/s13538-024-01667-9

[P017-2025] "Search for bottom quark associated production of the standard model Higgs boson in final states with leptons in proton-proton collisions at √s=13 TeV"

Hayrapetyan, A.; Tumasyan, A.; Adam, W.; **Chinellato, J. A.*;** et al.
CMS Collaboration

This Letter presents the first search for bottom quark associated production of the standard model Higgs boson, in final states with leptons. Higgs boson decays to pairs of tau leptons and pairs of leptonically decaying W bosons are considered. The search is performed using data collected from 2016 to 2018 by the CMS experiment in proton-proton collisions at a centre--of-mass energy of 13 TeV, corresponding to an integrated luminosity of 138 fb(-1). Upper limits at the 95% confidence level are placed on the signal strength for Higgs boson production in association with bottom quarks; the observed (expected) upper limit is 3.7 (6.1) times the standard model prediction.

PHYSICS LETTERS B 860, 139173, 2025. DOI: 10.1016/j.physletb.2024.139173

[P018-2025] "Seesaw limit of the Nelson-Barr mechanism"

Cherchiglia, A. L.*; Dias, A. G.; Leite, J.; Nishi, C. C.

We investigate how the solution to the strong CP problem and the explanation for the observed fermion mass hierarchies can be intrinsically related. Specifically, we explore the Nelson-Barr mechanism and identify its "seesaw limit", where light quark masses are suppressed by large CP-violating terms. Upon adding three (two) vector-like quarks that mix with the down-type (up--type) quark sector of the Standard Model, we demonstrate how the lack of CP violation in the strong sector and the observed quark mass hierarchy can be simultaneously achieved.

PHYSICS LETTERS B 860, 139222, 2025. DOI: 10.1016/j.physletb.2024.139222

[P019-2025] "Stimulating neuroplasticity: Therapeutic applications of an extended digital musical instrument"

Partesotti, E.; **Feitosa, J. A.***; Manzolli, J.; **Castellano, G.***

IntroductionMusic therapy has been widely applied to aid individuals both psychologically and physically, including as rehabilitation training for stroke patients. Recently, the use of novel technologies such as Digital Musical Instruments (DMIs) and Virtual Reality (VR) has become more common in this field. To broaden the application of music therapy with these technologies to neurological patients, it is important to understand their effects on the brain.MethodThe aim of this propositional study is to present a quantitative evaluation of brain network changes, using functional Magnetic Resonance Imaging (fMRI), occurring in individuals who used an XR-based Extended DMI (EDMI), namely, BehCreativeBehCreative is an immersive EDMI that provides sound and visual feedback based on the user's body movements. Five healthy individuals underwent ten training sessions with BehCreative and resting-state fMRI scans (before the first and after the last session). Results Functional connectivity changes between those scans were examined. A strengthened connection between brain areas associated with movement and audiovisual feedback processing was identified, possibly associated with an increase in motivation and cognitive engagement during audio-visual tasks. In general, connectivity changes pointed to an increase in arousal in the tested subjects, which may have been linked to the activation of the reward system during the use of the EDMI. DiscussionThese results are in line with our initial hypothesis, which was that training with BehCreative stimulates the neuroplasticity of the reward system. This study builds upon our previous research, on the therapeutic potential of DMIs.

NORDIC JOURNAL OF MUSIC THERAPY 34[1], SI, 62-80, 2025. DOI: 10.1080/08098131.2024.2445824

[P020-2025] "Synthesis and characterization of proton--conductive [GO-CoFe 2 O 4 @γ-Fe 2 O 3] nanocomposites series for impedimetric olfaction of clinically relevant VOCs in simulated human breath"

Albuquerque, L. E.; Junior, T. A.; Gomide, G.; Depeyrot, J.; Campos, A. F. C.; Vercillo, O. E.; Rodrigues, A. M.; Neto, B. G. E.; **Landers, R.***; Silva, S. W. da; Silva, G. F. B. L. e; Silva, M. F. P. da

In the pursuit of non-invasive breath biopsy technique development, we synthesized a series of proton- conductive [GO--CoFe2O4@gamma-Fe2O3] nanocomposites as sensing materials for electronic olfaction to detect and quantify clinically relevant VOC biomarkers in the human breath vapor approximation. Extensive characterization (TG, XRD, SEM, TEM, Raman, EIS, XPS) confirmed the proton conductivity character of materials as the primary sensing mechanism. The progressive doping of GO with CoFe2O4@gamma-Fe2O3 nanoparticles give rise to orthogonality of the impedimetric sensor array, allowing for the effective discrimination of VOCs over 2 orders of magnitude (20-1000 ppm), at room temperature and 80 % R.H.

MATERIALS CHEMISTRY AND PHYSICS 333, 130307, 2025. DOI: 10.1016/j.matchemphys.2024.130307

[P021-2025] "Synthesis and Magnetic Characterization of Dispersed FexNi100-x (x=10, 20, 30, 40, and 50) Nanoalloys Using the Thermal Decomposition Method"

Peixoto, E. B.; Andrade, L. F. S.; **Carvalho, M. H.***; Santos, J. D. T.; Silva, L. S.; Duque, J. G. S.

In this paper, we report on synthesis and magnetic properties of dispersed FexNi1-x (x = 10, 20, 30, 40, and 50) nanoalloys grown by thermal decomposition. X-ray diffraction patterns show that the majority crystalline phase is consistent with a fcc crystal structure (space group Fm3m) for all samples. Magnetization as a function of magnetic field and temperature shows that FexNi1-x are superparamagnetic with blocking temperatures around 10 K. However, for all samples, it is possible to observe a second very broad maximum, which can be ascribed to a bimodal nanoparticle size distribution and/or Ni nanoparticles for the case of samples grown with x = 10, 20, and 30. Finally, we argue that the nanoalloy size distribution and/or interaction effects should play a crucial role in determining the magnetic behavior of samples once we are not able to fit our HC(T) data using the Neel relaxation and the Bean-Livingston approaches in a wide temperature range.

BRAZILIAN JOURNAL OF PHYSICS 55[1], 41, 2025. DOI: 10.1007/s13538-024-01679-5

[P022-2025] "THOR: Inclusion of charge carriers' creation and transport in semiconductor detectors in the PENELOPE Monte Carlo simulation code"

Mendes, H. R.*; Tomal, A.*

This study introduces the simulation framework THOR, which was designed to include the creation and transport of electrons and holes in pixelated semiconductors detectors used for x--ray imaging in the PENELOPE v. 2014 Monte Carlo code and its penEasy v.2015 extension. Following the simulation of radiation transport and energy deposition in the detector, the THOR code breaks down into electron-hole pair (EHP) creation, transport, trapping, and modes of detection, including simulations of energy integrating and photon counting detectors. Validation of the THOR code was conducted using the ARTEMIS code. This study shows the impact of the simulation parameters (detector geometry, photon energy, charge carrier dispersion, etc.) on the detector performance metrics. Notably, the energy cut-off for transport of electrons and photons were found to significantly influence accuracy and computational speed, with the identification of the optimal value as 250 eV for improved computational performance without sacrificing accuracy. The ability to adjust the energy necessary to create an EHP specifically for a-Se sensors introduce a novel approach to balancing speed and accuracy effectively. Moreover, the THOR code allows the user to choose the bias direction and which charge is collected, showing the code's adaptability across various operational scenarios and materials. For instance, the results showed that using a negative bias and collecting holes results in a worst spatial resolution because the charge would have to travel a longer distance to be collected. Additionally, since the probability of trapping increases with the distance traveled by the charge carrier, trapping becomes a more significant factor in detection simulations for longer distances. The inclusion or exclusion of charge trapping in simulations can significantly influence the detector efficiency, with differences up to 60%. Analysis of physical parameters such as photon energy, detector thickness, composition, and applied electric field provides insights into their effects on detector performance metrics. Understanding these effects is essential for optimizing imaging systems for specific applications, thereby advancing diagnostic capabilities and patient care in medical imaging. In summary, this study offers a comprehensive understanding of detector behavior and simulation optimization, aiming to enhance imaging techniques.

RADIATION PHYSICS AND CHEMISTRY 229, 112437, 2025. DOI: 10.1016/j.radphyschem.2024.112437

[P023-2025] "Tripartite state characterization via activated bipartite entanglement"

Arruda, L. G. E.*; Balthazar, W. F.; **Moreira, M. V.*;** Passos, M. H. M.; Huguenin, J. A. O.; **Oliveira, M. C. de***

We propose a procedure to identify and classify genuine tripartite entanglement in pure 3-qubit states via the Activated Bipartite Entanglement (ABE), which is defined here as the difference between the Entanglement of Assistance and the Entanglement of Formation. We show that for pure states belonging to one of the two inequivalent classes of genuine tripartite entanglement, i.e., GHZ or W states, the ABE is always greater than zero. For separable and biseparable states it is always null. In addition, our approach is capable to distinguish between genuine tripartite entangled states, those belonging to the GHZ-class from those belonging to the Wclass. We also present an experimental proposal, by using linear optical circuits and internal degrees of freedom of a single photon, to measure the ABE and to verify the characterization via activated entanglement. The circuit simulation shows an excellent agreement with theoretical prediction for a wide class of GHZ and W states.

PHYSICS LETTERS A 535, 130223, 2025. DOI: 10.1016/j.physleta.2025.130223

[P024-2025] "Widely tunable dual acousto-optic interferometric device based on a hollow core fiber"

Silva, R. E. da*; Osorio, J. H.; Gerome, F.; Benabid, F.; Webb, D. J.; Franco, M. A. R.; **Cordeiro, C. M. B.***

An all-fiber, dual Mach-Zehnder interferometer (MZI) based on an acoustically modulated hollow core fiber (HCF) is experimentally demonstrated for the first time. By attaching an acoustic driver between the fixed ends of an HCF, we fabricated two acousto-optic modulators (AOMs) with distinct driver positions, allowing synchronization of two in-line MZIs inside the HCF. The first MZI is set by two acoustic long-period gratings separated by a second MZI formed at the fiber and driver-attaching region. We show that this setup enables frequency-tuning of the coupling between the fundamental and higher-order modes in the HCF. Additionally, we simulate and analyze the HCF modal couplings and MZIs' modulated spectra under distinct device parameters using the transfer matrix method. The new AOM-MZI enables tuning of the MZI's free spectral range by adjusting 1 Hz of the electrical frequency, which is promising to modulate multiwavelength filters, sensors, and fiber lasers.

OPTICS AND LASER TECHNOLOGY 182, 112093, 2025. DOI: 10.1016/j.optlastec.2024.112093

[P025-2025] "X-ray photoelectron diffraction as one efficient tool for surface structure determination of corrugated 2D materials"

Lima, L. H. de; **Siervo, A. de***

This brief review discusses the application of X-ray photoelectron diffraction (XPD) as an effective experimental tool for determining the surface structure of two-dimensional (2D) corrugated materials, such as graphene and hexagonal boron nitride. XPD stands out for its ability to provide precise atomic positions, interlayer distances, bond lengths, and bond angles. Such detailed experimental data are essential for refining theoretical models and complement the findings obtained through other techniques, like scanning probe microscopy (SPM). This brief review includes examples of surface structure studies on sp2-hybridized corrugated monolayers, such as graphene on Ir(111), Fe-intercalated graphene on Ir(111), hBN on Rh(111), and graphene on SiC(0001). XPD has uncovered significant structural details, such as corrugation amplitude and adsorption distances to the substrate, contributing to an enhanced understanding of the electronic, mechanical, optical, magnetic, and physicochemical properties of 2D materials.

SURFACE SCIENCE 754, 122683, 2025. DOI: 10.1016/j.susc.2024.

***Autores da comunidade IFGW**
Fonte: Web of Science on-line (WOS)

Defesas de Dissertações do IFGW

[D002-2025] "Não-classicalidade de Bell em redes: limitando o conjunto de correlações clássicas"
Aluno: Pedro Nobrega Lauand
Orientador: Prof. Dr. Rafael Luiz da Silva Rabelo
Data: 18/02/2025

[D003-2025] "Relações entre não-localidade de Bell e contextualidade de Kochen-Specker"
Aluno: Lucas Emanuel Antunes Porto
Orientador: Prof. Dr. Marcelo de Oliveira Terra Cunha
Data: 18/02/2025

[D004-2025] "Propriedades e estruturas dos grafinos e seus derivados: Um estudo computacional"
Aluno: Guilherme Brunharo Kanegae
Orientador: Prof. Dr. Alexandre Fontes da Fonseca
Data: 20/02/2025

[D005-2025] "Combinação de TD-DFT e Pixel Counting Method para determinação de seção de choque de captura eletrônica para prótons colidindo em moléculas orgânicas"
Aluno: Luca Aguiar de Oliveira
Orientador: Prof. Dr. Mario Antonio Bernal Rodriguez
Data: 24/02/2025

Defesas de Teses do IFGW

[T002-2025] "Opto-Eletro-Mecânica em Niobato de Lítio"
Aluno: Caique Conde Rodrigues
Orientador: Prof. Dr. Gustavo Silva Wiederhecker
Data: 27/02/2025

[T003-2025] "Supercondutividade e Ferromagnetismo Não Convencionais em Bismuto Elementar"
Aluno: Carlos Alberto Invernezzi Canhassi
Orientador: Prof. Dr. Iakov Veniaminovitch Kopelevitch
Data: 28/02/2025

[T004-2025] "Aplicações de Conectividade Funcional na Avaliação de Distúrbios Neurológicos"
Aluno: Bruna Mezzari Carlos
Orientador: Profa. Dra. Gabriela Castellano
Data: 06/03/2025

Fonte: Portal IFGW/Eventos
Disponível em: https://portal.ifi.unicamp.br/a-instituicao/eventos/month.calendar/2023/12/14/-

Defesas de Dissertações e Teses do PECIM

***Sem atualização na página no período**
Fonte: Página do PECIM
Disponível em: https://www.pecim.unicamp.br/bancas

Cadastre-se no site do Boletim Abstracta como leitor, e receba os avisos da publicação de novos números por e-mail.

Abstracta

Instituto de Física
Diretor: Profa. Dra. Mônica Alonso Cotta
Diretora Associada: Prof. Dr. Marcos Cesar de Oliveira
Universidade Estadual de Campinas - UNICAMP
Cidade Universitária Zeferino Vaz
13083-859 - Campinas - SP - Brasil
e-mail: secdir@ifi.unicamp.br
Fone: +55 19 3521-5300

Publicação

Biblioteca do Instituto de Física Gleb Wataghin
http://portal.ifi.unicamp.br/biblioteca
Instagram: @bif.unicamp

Diretora Técnica: Sandra Maria Carlos Cartaxo
Coordenadora da Comissão de Biblioteca: Profa. Dra. Arlene Cristina Aguilar

Elaboração e editoração:
Maria Graciele Trevisan (Bibliotecária)
Amelia Galdino Monteiro Amancio (Técnica)

Contato: infobif@ifi.unicamp.br